differentiation of human epidermal keratinocytes. J. Invest. Dermatol. 120, 1007–1015.
Gröne, A., 2002. Keratinocytes and cytokines. Vet. Immunol. Immunopathol. 88, 1–12.
Hisadome, K., Koyama, T., Kimura, C., Droogmans, G., Ito, Y., Oike, M., 2002. Volume-regulated anion channels serve as an auto/paracrine nucleotide release pathway in aortic endothelial cells. J. Gen. Physiol. 119, 511–520.
Inoue, K., Hosoi, J., Denda, M., 2007. Extracellular ATP has stimulatory effects on the expression and release of IL-6 via purinergic receptors in normal human epidermal keratinocytes. J. Invest. Dermatol. 127, 362–371.
Ishimaru, M., Tsukimoto, M., Harada, H., Kojima, S., 2013. Involvement of $P2Y_{11}$ receptor in IFN-γ-induced IL-6 production in human keratinocytes. Eur. J. Pharmacol. 703, 67–73.
Kawakami, M., Kaneko, N., Anada, H., Terai, C., Okada, Y., 1997. Measurement of interleukin-6, interleukin-10, and tumor necrosis factor-alpha levels in tissues and plasma after thermal injury in mice. Surgery 121, 440–448.
Kirnbauer, R., Kock, A., Schwarz, T., Urbanski, A., Krutmann, J., Borth, W., Damm, D., Shipley, G., Ansel, J.C., Luger, T.A., 1989. IFN-beta 2, B cell differentiation factor 2, or hybridoma growth factor (IL-6) is expressed and released by human epidermal cells and epidermoid carcinoma cell lines. J. Immunol. 142, 1922–1928.
Kirnbauer, R., Kock, A., Neuner, P., Förster, E., Krutmann, J., Urbanski, A., Schauer, E., Ansel, J.C., Schwarz, T., Luger, A., 1991. Regulation of epidermal cell interleukin-6 production by UV light and corticosteroiods. J. Invest. Dermatol. 96, 484–489.
Kock, A., Schwarz, T., Kirnbauer, R., Urbanski, A., Perry, P., Ansel, J.C., Luger, T.A., 1990. Human keratinocytes are a source for tumor necrosis factor α: evidence for synthesis and release upon stimulation with endotoxin or ultraviolet light. J. Exp. Med. 172, 1609–1614.
Koegel, H., Alzheimer, C., 2001. Expression and biological significance of Ca^{2+}-activated ion channels in human keratinocytes. FASEB J. 15, 145–154.
Koizumi, S., Fujishita, K., Inoue, K., Shigemoto-Mogami, Y., Tsuda, M., Inoue, K., 2004. Ca^{2+} waves in keratinocytes are transmitted to sensory neurons: the involvement of extracellular ATP and P2Y2 receptor activation. Biochem. J. 380, 329–338.
Kondo, S., Kono, T., Sauder, D.N., McKenzie, R.C., 1993. IL-8 gene expression and production in human keratinocytes and their modulation by UVB. J. Invest. Dermatol. 101, 690–694.
Lazarowski, E.R., Boucher, R.C., Harden, T.K., 2000. Constitutive release of ATP and evidence for major contribution of ecto-nucleotide pyrophosphatase and nucleoside diphosphokinase to extracellular nucleotide concentrations. J. Biol. Chem. 275, 31061–31068.
Luo, X., Morrin, A., Killard, A.J., Smyth, M.R., 2006. Application of nanoparticles in electrochemical sensors and biosensors. Electroanalysis 4, 319–326.
Manke, A., Wang, L., Rojanasakul, Y., 2007. Mechanisms of nanoparticle-induced oxidative stress and toxicity. BioMed Res. Int. 2013, 942916, http://dx.doi.org/10.1155/2013/942916 (15 p.).
Medina, C., Santos-Martinez, M.J., Radomski, A., Corrigan, O.I., Radomski, M.W., 2007. Nanoparticles: pharmacological and toxicological significance. Br. J. Pharmacol. 150, 552–558.
Mizumoto, N., Mummert, M.E., Shalhevet, D., Takashima, A., 2003. Keratinocytes ATP release assay for testing skin-irritating potentials of structurally diverse chemicals. J. Invest. Dermatol. 121, 1066–1072.
Napierska, D., Thomassen, L.C.J., Lison, D., Martens, J.A., Hoet, P., 2010. The nanosilica hazard: another variable entity. Part. Fibre Toxicol. 7, 39.
Neuner, P., Urbanski, A., Trautinger, F., Moller, A., Kirnbauer, R., Kapp, A., Schopf, E., Schwarz, T., Luger, T.A., 1991. Increased IL-6 production by monocytes and keratinocytes in patients with psoriasis. J. Invest. Dermatol. 97, 27–33.
Ohshima, Y., Tsukimoto, M., Takenouchi, T., Harada, H., Suzuki, A., Sato, M., Kitani, H., Kojima, S., 2010. Gamma-irradiation induces P2X(7) receptor-dependent ATP release from B16 melanoma cells. Biochim. Biophys. Acta 1800, 40–46.
Pankratov, Y., Lalo, U., Verkhratsky, A., North, R.A., 2006. Vesicular release of ATP at central synapses. Pflugers Arch. 452, 589–597.
Partridge, M., Chantry, D., Turner, M., Feldmann, M., 1991. Production of interleukin-1 and interleukin-6 by human keratinocytes and squamous cell carcinoma cell lines. J. Invest. Dermatol. 96, 771–776.
Pastore, S., Mascia, F., Gulinelli, S., Forchap, S., Dattilo, C., Adinolfi, E., Girolomoni, G., Di Virgilio, F., Ferrari, D., 2006. Stimulation of purinergic receptors modulates chemokine expression in human keratinocytes. J. Invest. Dermatol. 127, 660–667.
Pellegatti, P., Falzoni, S., Pinton, P., Rizzuto, R., Di Virgilio, F., 2005. A novel recombinant plasma membrane-targeted luciferase reveals a new pathway for ATP secretion. Mol. Biol. Cell 16, 3659–3665.
Sabirov, R.Z., Dutta, A.K., Okada, Y., 2001. Volume-dependent ATP-conductive large-conductance anion channel as a pathway for swelling-induced ATP release. J. Gen. Physiol. 118, 251–266.
Schwarz, T., Luger, T.A., 1989. Effect of UV irradiation on epidermal cell cytokine production. J. Photochem. Photobiol. B 4, 1–13.
Sprague, R.S., Ellsworth, M.L., Stephenson, A.H., Kleinhenz, M.E., Lonigro, A.J., 1998. Deformation-induced ATP release from red blood cells requires CFTR activity. Am. J. Physiol. 275, 1726–1732.
Stout, C.E., Costantin, J.L., Naus, C.C., Charles, A.C., 2002. Intercellular calcium signaling in astrocytes via ATP release through connexin hemichannels. J. Biol. Chem. 277, 10482–10488.
Tsukimoto, M., Homma, T., Ohshima, Y., Kojima, S., 2010. Involvement of purinergic signaling in cellular response to gamma radiation. Radiat. Res. 173, 298–309.
Uratsuji, H., Tada, Y., Kawashima, T., Kamata, M., Hau, C.S., Asano, Y., Sugaya, M., Kadono, T., Asahina, A., Sato, S., Tamaki, K., 2012. P2Y6 receptor signaling pathway mediates inflammatory responses induced by monosodium urate crystals. J. Immunol. 188, 436–444.
Urbanski, A., Schwarz, T., Neuner, P., Krutmann, J., Kirnbauer, R., Kock, A., Luger, T.A., 1990. Ultraviolet light induces increased circulating interleukin-6 in humans. J. Invest. Dermatol. 94, 808–811.
Uskoković, V., 2013. Entering the era of nanoscience: time to be so small. J. Biomed. Nanotechnol. 9, 1441–1470.
Wilkin, F., Duhant, X., Bruyns, C., Suarez-Huerta, N., Boeynaems, J.M., Robaye, B., 2001. The P2Y11 receptor mediates the ATP-induced maturation of human monocyte-derived dendritic cells. J. Immunol. 166, 7172–7177.
Xia, T., Kovochich, M., Brant, J., Hotze, M., Sempf, J., Oberley, T., Sioutas, C., Yeh, J.I., Wiesner, M.R., Nel, A.E., 2006. Comparison of the abilities of ambient and manufactured nanoparticles to induce cellular toxicity according to an oxidative stress paradigm. Nano Lett. 6, 1794–1807.
Yang, W., Peters, J.I., William III, R.O., 2008. Inhaled nanoparticles—a current review. Int. J. Pharm. 456, 239–247.
Yoshida, H., Kobayashi, D., Ohkubo, S., Nakahata, N., 2006. ATP stimulates interleukin-6 production via P2Y receptors in human HaCaT keratinocytes. Eur. J. Pharmacol. 540, 1–9.
Zhang, G., Zeng, X., Li, P., 2013. Nanomaterials in cancer-therapy drug delivery system. J. Biomed. Nanotechnol. 9, 741–750.

大気中の小さな粒子（$PM_{2.5}$）による健康影響を防ぐために

梅澤　雅和

東京理科大学　薬学部　衛生化学研究室
東京理科大学　総合研究機構　戦略的環境次世代健康科学研究基盤センター

$PM_{2.5}$の現状

$PM_{2.5}$とは、大気中の浮遊粒子状物質（SPM: suspended particulate matter）のうち直径が2.5 μm以下の微小粒子の総称です。SPMのうち、とくに微小な粒子が健康影響に大きく寄与していることが明らかになり、大気中濃度の監視・記録と環境基準値の設定が行われています。日本では、2001年から大気中の$PM_{2.5}$のモニターが始まり、2009年に$PM_{2.5}$の環境基準値(*1)が策定されました。

(*1) 日本における PM2.5 の環境基準値は、「1年平均値が15 μg/m^{3}以下であり、かつ、1日平均値が35 μg/m^{3}以下」と定められています。(2014年2月現在)

2013年1月以来、日本国内で微小粒子$PM_{2.5}$の問題が、頻度高くマスコミに取り上げられています。突然に報道が多くなった理由は、日本の$PM_{2.5}$濃度が2012年以前よりも著しく高くなったからではありません。2012年末に中国における$PM_{2.5}$濃度が公開され、現地での著しい高い値が報道されたことにより注目を集めたことが、その背景にあります。

中国では、例えば北京の$PM_{2.5}$濃度が、冬季には頻繁に100 μg/m^{3}を大きく超えるという深刻な状況です[1]。現在の日本で、$PM_{2.5}$濃度が100 μg/m^{3}に達することは稀です。ただし、$PM_{2.5}$濃度の1日平均値や年平均値が環境基準値を超える例は、今の日本でも少なからず起こっています。国内の一般大気環境についての$PM_{2.5}$の環境基準達成率は、2010年度の時点でも32.4%（34地点中11地点）に過ぎません。今後、健康影響を防ぐための新たな対策が取られる必要があると言えるでしょう。

一方で$PM_{2.5}$についての最近の報道は、中国大陸からの越境汚染に強い関心を引きつける内容が多いように思われます。しかし、実際には国内の$PM_{2.5}$のうち越境汚染によるものは一部に過ぎず、大部分は国内で発生したものであることに注意が必要です。

$PM_{2.5}$の健康影響（疫学的な知見）

SPMによる健康影響が注目されるきっかけとなった代表的な事例の一つに、1950年代に起こったロンドンスモッグがあります。この直後の1958年から、ロンドンにおける大気汚染による健康影響が疫学的に研究されました。その結果、大気中SPM濃度と1日あたりの死亡者数との間に正の相関があることが示されたのです[2]。これは、高濃度のSPMが循環器系や呼吸器系に影響を及ぼし、主に心筋梗塞や呼吸器疾患の発作を引き起こしたことにより生じたと考えられています。

その後、SPMのうちでも比較的小さな$PM_{2.5}$が、この死亡者数の増加に大きく関わることが明らかになりました[3]。さらに、高齢者、小児、胎児や、循環器系もしくは呼吸器に疾病を持つ人、および重度の肥満や糖尿病を罹患している人であることも、複数の疫学研究により示されています[4]。日本では2013年2月末から、昼間の$PM_{2.5}$濃度が70 μg/m^{3}以上に達すると予測される日に、注意喚起がなされるようになりました。この注意喚起が出たときには、とくに循環器および呼吸器の疾患や糖尿病を持つ人たちの生活環境に注意すべきと言えると思われます。

$PM_{2.5}$のデータを見るときの注意点

私たちが$PM_{2.5}$による健康影響を防ぐためには、関連する情報を一人一人が理解し、各々の事情にあわせた対応を取ることが求められることもあることでしょう。そのような場面で$PM_{2.5}$濃度のデータを解釈する際に、心に留めていただきたい点を次の3つにまとめました。

1. 日平均値なのか、年平均値なのか
2. ゼロになるものではないこと
3. 他の時季の同地点の数値と比べてどの程度か

大気中のSPM濃度や$PM_{2.5}$濃度は、もともと日内変動の大きいものです。そのため、たとえば同じ「45 μg/m^3」という数値でも、それが一時的に（例えば、ある1時間だけ）その濃度であることと、1日平均としてその濃度であることと、1年間の平均値としてその濃度であることとでは、各々まったく意味が異なります。45 μg/m^{3}が1日平均値であるとなると、環境基準値（35 μg/m^3）を超えた高値ということになります。しかし、$PM_{2.5}$濃度は気象条件や産業活動により大きく変動します。そのため、$PM_{2.5}$濃度が45 μg/m^{3}になったのがある1時間の間だけであった場合には、それは頻繁に起こることであり、これに対策をするのは現時点では現実的でないと言うことができます。

しかし、残念ながら現在は、$PM_{2.5}$濃度がマスコミで報道されるときなどに、その値が上のいずれの平均値であるのか示されない場合がほとんどです。$PM_{2.5}$の人への曝露量は「濃度×時間」で表されます。そこで、私たちはその「濃度」の数値だけにとらわれず、それが一時的なものなのか、長期的に続いているものなのかを確認することが望ましいのです。あわせて、大気環境中の$PM_{2.5}$は決してゼロにはならないことも理解する必要があります。$PM_{2.5}$には産業活動に伴う燃焼だけでなく、自然界の中で発生するものもあります。そのため、いくら曝露量を減らすのが良いと言っても、その濃度をゼロにすることは現実にはできないのです。

また、$PM_{2.5}$濃度には季節差や地域差もあります。そのため、ある時点での$PM_{2.5}$濃度の値を見たときにそれが「以前よりも増えたのか減ったのか」を知るためには、同時季の同時点での値と比較してどうなのかを検証する必要があります。たとえば、日本における$PM_{2.5}$濃度は、3～5月の春季において黄砂の影響を受け、他の季節と比べて高くなる傾向にあります。これは、$PM_{2.5}$の越境汚染が頻繁にマスコミで報道された2013年も同様でした。$PM_{2.5}$に関するマスコミの報道は、中国国内で$PM_{2.5}$の著しい高濃度が頻発した1～2月に大変多かったのですが、一方の日本国内で$PM_{2.5}$濃度が高かったのは、この年も3～5月であったことが分かっています。

また、地域差については、長期的に見ると黄砂を受けやすい西日本の方が、東・北日本と比べて$PM_{2.5}$濃度が高いことが分かっています。ある地点での$PM_{2.5}$の増減の推移を知るためには、その地点での過去のデータが必要になるということがお分かりいただけるでしょうか。

さらに、最近では$PM_{2.5}$の中でも、$PM_{0.1}$とも呼ぶべきとくに小さな（ナノサイズの）粒子が、独特かつ大きな健康影響を及ぼす可能性があることが指摘されており[5]、私たちもその健康影響を理解し、防止策を講じるための研究を進めているところです。

ではどうすればいいのか—有害影響を避けるために

以上を踏まえた上で、「それでは、私たち一人一人が$PM_{2.5}$の有害影響を避けるために、どうすることが現実的でかつ有効なのか」を述べたいと思います。

まず、幹線道路、バスやトラックなどのターミナル、タバコの煙のある空間にいる時間を短くすることが有効です。そのような場所に行かないことはできずとも（ゼロにはできなくても）、そこに滞在する時間を少なくする（曝露量を減らす）ことが有効であるためです。

仕事柄、道路やターミナルで長時間仕事をする必要のある方々には、マスクを着用するなどの対策をとることも有効です。マスクでは$PM_{2.5}$や$PM_{0.1}$のすべてをカットできないという指摘もありますが、少なくとも一部がカットできることが明らかになっています。曝露量をゼロにはできなくても、曝露量を減らすことがリスクの回避には有効なのです。

本講演の内容が、皆様や周りの方々の不安の解決に少しでもつながり、健康を守るための行動選択の一助になれば幸いです。

謝辞

一連の研究は、武田健教授、柳田信也助教、立花研助教をはじめ、東京理科大学 薬学部 衛生化学研究室の方々のご支援をいただき実施しました。また、日本学術振興会・科学研究費補助金・若手研究（B）［24790130］（梅澤、2012～13年度）ならびに私立大学戦略的研究基盤形成支援事業「環境と次世代健康科学－疾患原因解明と予防に向けた先進的研究」（代表＝武田健、2011～2015年度）の助成をいただき研究を遂行しています。

参考文献

[1] 岡崎雄太：　広州市の大気汚染について -微小粒子状物資“$PM_{2.5}$”とは-、「大気汚染に関する講演会」資料（2013年3月12日）

[2] Schwartz and Marcus: Mortality and air pollution in London: a time series analysis. Am J Epidemiol 131: 185-94 (1990)

[3] Dockery et al.: An association between air pollution and mortality in six U.S. cities. N Engl J Med 329: 1753-1759 (1993)

[4] EPA (米国環境保護庁) Integrated science assessment for particulate matter.（2012年12月）

[5] 朝日新聞：　超微粒子、母体→胎児の脳へ　マウス実験、細胞に異常も（2013年10月29日）

＋　＋　＋

プロフィール

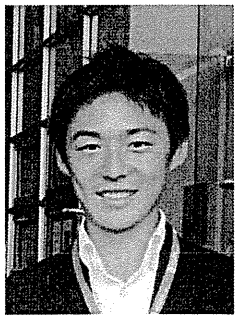

1983年福岡県生まれ、茨城県で育つ。ナノ粒子を始めとした環境要因および遺伝要因、栄養摂取や運動と健康状態との複雑な関係性を研究しながら、「科学的知見を人の生活に効果的に活かすためのプロセス」に強い関心を持っています。

東京理科大学 薬学部・助教。2006年に東京理科大学 薬学部を卒業し、薬剤師免許取得。2010年に東京理科大学大学院薬学研究科 博士課程を修了。同大学総合研究機構 PD 研究員、助教を経て、2013年4月より現職。

リスクコミュニケーション手法の改善の取り組みと教育プロセス

○梅澤　雅和[1,2]、難波　美帆[3,4]、石村　源生[5]

[1] 東京理科大学　総合研究機構　戦略的環境次世代健康科学研究基盤センター
[2] 東京理科大学　薬学部　衛生化学研究室
[3] 早稲田大学　早稲田大学大学院　政治学研究科　ジャーナリズムコース [J-SCHOOL]
[4] 現：　北海道大学　創成研究機構　URA ステーション
[5] 北海道大学　高等教育推進機構　高等教育研究部　科学技術コミュニケーション教育研究部門 [CoSTEP]

研究の背景

我々は日常生活の中で、様々な要因がもたらす危険性（リスク）に向き合っている。リスクに効果的に対応するためには、それに関わる情報が効果的に伝達・共有（リスクコミュニケーション）される必要がある。リスクコミュニケーションは、聞き手の行動変容を促しリスク回避が実現することで効果を発揮する。しかし、2011 年 3 月に発生した福島原子力発電所事故後の例のように、政府やマス・メディアが行うものも含め、リスクコミュニケーションは必ずしもうまくいかないことが多い。この事実は、リスクに関して社会に存在する葛藤や論争を解決できるコミュニケーションとは何かという課題を提示している。とくに、幼少児の健康に及ぶ環境リスクには社会的論争を招きやすく、十分な注意をして対処すべき課題の一つである。

一方で先行研究において、リスクコミュニケーションに際する情報提供者のリテラシーが問われることはなかった。本研究では、情報提供者が抱えるこのリテラシーの限界に起因する不安や懸念に注目した。とくに、あるコミュニケーション手法を取ることによりメリットとデメリットが生じ、不安や懸念に対する対処をしづらい場面を「ジレンマ状況」として焦点を当てた。

研究目的

本研究は、リスクコミュニケーションに際して遭遇し得るジレンマ状況を、パターン・ランゲージの手法を用いて形式知化することを目的として実施した。あわせて、この形式知化をワークショップ形式で行うことにより、集団内の経験知・暗黙知を形式知化するプロセスを参加者に体験してもらった。それにより、様々な立場の人が各々の目的に合う形でパターン集を作成するプロセスの、プロトタイプを提示することを目指した。

方法

パターン抽出のためのワークショップの設計と遂行

本研究では、リスクコミュニケーションの場面で繰り返し起こりうる類型的・普遍的な問題やジレンマ状況のパターンを抽出し、列挙することを目的とした。ジレンマ状況は、次のような特徴を持つものと定義した。

- 容易に解決しがたい。
- 分野をまたいだ共通点がある。
- それぞれの解決手法にはメリットとデメリットがある。

その目的を果たすために、本研究では「文脈、問題、対処案」をリスクコミュニケーションに際するジレンマ状況のパターンとし、次のフォーム（図）を作成し、ワークで使用した。

- 文脈
  - リスクコミュニケーション場面を規定する前提条件
  - 「何についてのリスクか」「リスクの情報源は誰か」など
- 問題
  - リスクコミュニケーション担当者の立場に立ったとき、上記文脈のもとで起こり得る様々な問題
- 対処案
  - 問題を解決ないし緩和するための対処案
  - その対処案を採用した場合に結果として起こることが想定される、メリットとデメリット

リスクの情報提供者の遭遇し得るジレンマ状況の形式知化は、リスクコミュニケーションを学ぶ早稲田大学大学院集中演習の中で、ジャーナリズムコースの学生と、一般社団法人サイエンス・メディア・センター（SMC）夏期集中ワークショップへの参加者の協力の下に、3 日間（2012 年 8 月 10 日～12 日）のワークショップ形式で実施した。

ワークショップの学習目標と達成度評価

本ワークショップにおいては、参加者に以下の 3 点を達成してもらうことを学習目標とした。

a) リスクコミュニケーションには必ずしも正解のないジレンマ状況があることを理解してもらうこと。
b) グループワークによって、上記のジレンマ状況を横断的に見渡した時に見られる共通の形式（＝「パ

ターン・ランゲージ」）を抽出すること。
c) 自らの経験からリスクコミュニケーションのジレンマ状況を抽出し形式知化する、抽象化スキルを獲得してもらうこと。

あわせて、ワークショップ参加者の学習に関する達成度を以下の項目により評価した。

A) リスクコミュニケーションについての理解を深めることができたか。
B) 多様なリスクコミュニケーション場面に対応できる「構え」を身につけることができたか。

結果

ワークショップには、研究者、ジャーナリスト、大学院生、科学コミュニケーターの計18名（ワーク前半［2日目、ワーク1日目］は20名）が参加した。3日間のワークショップの後、語の用法やパターンとしての文章形態を統一し、結果として51個のパターンが10個のグループに分けられる形で抽出された。グループは以下の10個となった。

1. 聞き手の理解を得られない
2. メディアの誤情報に対応できない
3. 社会の中での役割まで問われる
4. 意見や判断まで問われる
5. 情報伝達テクニックに不安がある
6. コミュニケーターの側にある問題
7. 信頼関係の問題
8. 情報が扱いづらい
9. 緊急時にリスクを伝える
10. コンテンツに依存したジレンマ状況

学習目標の達成度評価については、先に示した2つの評価項目に対して、本ワークショップは一定程度の成果を挙げることができた。一方で、リスクコミュニケーションのジレンマ状況のパターン化・可視化の試みを行ったことにより、同様の試みを行うときに起こり得る課題も明らかになった。とくに、このワークショップへの参加者らが様々な背景や経験を持っている状況で、1）ワークを通して何を抽出しようとしているのか、2）ジレンマ状況をどのようにパターン（問題や対処案）の中に表現するかを共有することは容易ではなかった。また、ワークショップを終えた時点では、「問題『価値観が違う』→「対処案『価値観をそろえる』」のように、対処案が問題を裏返しただけの記述になっているパターン・ランゲージが複数存在した。

考察

本ワークショップでは、参加者どうしが様々な立場や自らの体験を踏まえて、リスクコミュニケーションで生じ得るジレンマ状況の抽出を行った。それにより、実際にコミュニケーターや専門家がリスクの情報提供を行う場に臨むに際して、その場で取れ得るコミュニケーション手法を確認できるパターン集を作成することができた。ワークを通して参加者どうしが議論し合い、体験や考えやを共有したことで、暗黙知であったリスクコミュニケーションのジレンマ状況の形式知化は一定以上の成果を収めたと考えられる。今後、同様の試みが複数行われることにより、より全体を網羅したジレンマ状況の体系化が進むことが期待される。

また、ワークショップで得られたパターンの素案を推敲・校正するなどのフォローアップをしたり、同じような教育プロセスを繰り返し行ったりすることが有効であろう。とくに、幼少児の教育や保育の仕事に携わる人々は、環境が健康に及ぼすリスクを子ども自身や保護者に説明することを求められることが少なくない。そうした人々を交えて同様の試みが行われることで、幼少児の健康をより効果的に守っていくことができるのではないかと期待される。

結論

本研究では、社会に横たわる様々なリスクや葛藤と向き合うコミュニケーターがワークショップに集まり、リスクコミュニケーションで発生し得るジレンマ状況の抽出と共有を行うことができた。また、そのプロセスは参加者にとってリスクコミュニケーション手法を学べる学習効果を発揮した。

我々は誰しも、日常の仕事の中で、身の回りにあるリスクを説明し、情報提供を求められる場面に遭遇し得る。これは、子どもの健康や安全と向き合う教育・保育・スポーツクラブ等の現場で活躍する人々も例外ではない。今後、同様のリスクコミュニケーション手法のパターン抽出・形式知化の試みが様々なコミュニティにより繰り返し行われることにより人々に効果的な行動変容とリスク回避を促すコミュニケーション手法がより洗練された形で示されることを期待したい。

謝辞

本研究は、日本学術振興会・科学研究費補助金・若手研究（B）［24790130］（梅澤、2012～13年度）ならびに私立大学戦略的研究基盤形成支援事業「環境と次世代健康科学－疾患原因解明と予防に向けた先進的研究」（代表＝武田健、2011～2015年度）の支援を受けて遂行した。ワークショップの実施に際しては、早稲田大学東日本大震災復興研究拠点、先端環境医工科学研究所、先端科学・健康医療融合研究機構の支援をいただいた他、ファシリテーターとして浦山絵里様、菅野綾子様、高尾戸美様のご支援をいただいた。

OPEN ACCESS Freely available online

PLOS | ONE

Effects of Maternal Exposure to Ultrafine Carbon Black on Brain Perivascular Macrophages and Surrounding Astrocytes in Offspring Mice

Atsuto Onoda[1,2]*, Masakazu Umezawa[1,3], Ken Takeda[1,3], Tomomi Ihara[2], Masao Sugamata[2]

1 Department of Hygienic Chemistry, Faculty of Pharmaceutical Sciences, Tokyo University of Science, Noda, Chiba, Japan, **2** Department of Pathology, Tochigi Institute of Clinical Pathology, Nogi, Tochigi, Japan, **3** The Center for Environmental Health Science for the Next Generation, Research Institute for Science and Technology, Tokyo University of Science, Noda, Chiba, Japan

Abstract

Perivascular macrophages (PVMs) constitute a subpopulation of resident macrophages in the central nervous system (CNS). They are located at the blood-brain barrier and can contribute to maintenance of brain functions in both health and disease conditions. PVMs have been shown to respond to particle substances administered during the prenatal period, which may alter their phenotype over a long period. We aimed to investigate the effects of maternal exposure to ultrafine carbon black (UfCB) on PVMs and astrocytes close to the blood vessels in offspring mice. Pregnant mice were exposed to UfCB suspension by intranasal instillation on gestational days 5 and 9. Brains were collected from their offspring at 6 and 12 weeks after birth. PVM and astrocyte phenotypes were examined by Periodic Acid Schiff (PAS) staining, transmission electron microscopy and PAS-glial fibrillary acidic protein (GFAP) double staining. PVM granules were found to be enlarged and the number of PAS-positive PVMs was decreased in UfCB-exposed offspring. These results suggested that in offspring, "normal" PVMs decreased in a wide area of the CNS through maternal UfCB exposure. The increase in astrocytic GFAP expression level was closely related to the enlargement of granules in the attached PVMs in offspring. Honeycomb-like structures in some PVM granules and swelling of astrocytic end-foot were observed under electron microscopy in the UfCB group. The phenotypic changes in PVMs and astrocytes indicate that maternal UfCB exposure may result in changes to brain blood vessels and be associated with increased risk of dysfunction and disorder in the offspring brain.

Citation: Onoda A, Umezawa M, Takeda K, Ihara T, Sugamata M (2014) Effects of Maternal Exposure to Ultrafine Carbon Black on Brain Perivascular Macrophages and Surrounding Astrocytes in Offspring Mice. PLoS ONE 9(4): e94336. doi:10.1371/journal.pone.0094336

Editor: Michelle L. Block, Virginia Commonwealth University, United States of America

Received January 30, 2014; **Accepted** March 12, 2014; **Published** April 10, 2014

Funding: This work was supported in part by a JSPS KAKENHI Grant Number 24790130 (http://www.jsps.go.jp/english/e-grants/; 2012-2013), a MEXT-Supported Program for the Strategic Research Foundation at Private Universities (http://www.mext.go.jp/english/; 2011-2015) and a Grant-in-Aid for the Health and Labour Sciences Research Grant (Research on the Risk of Chemical Substances) from the Ministry of Health, Labour and Welfare (Grant Number 12103301, http://www.mhlw.go.jp/english/; 2012-2014). The funders had no role in study design, data collection and analysis, decision to publish, or preparation of the manuscript.

Competing Interests: The authors have declared that no competing interests exist.

* E-mail: atsutoyukari@gmail.com

Introduction

Resident phagocytes of the central nervous system (CNS) are categorized into four types: microglia, meningeal macrophages, choroid plexus macrophages, and perivascular macrophages (PVMs). These contribute to maintaining homeostasis in the CNS [1,2]. Recently initiated investigations aim to elucidate the characteristics and function of PVMs, also called perivascular cells, perivascular microglia and fluorescent granular perithelial cells [3]. PVMs are localized in the perivascular space (Virchow-Robin space) and are surrounded by the vascular endothelial basement membrane and glia limitans [4,5]. In this space, PVMs adjoin endothelial cells, pericytes [4,5,6], and the end-foot of astrocytes, which are one of the types of cerebral parenchyma glial cells in the surrounding brain microvessels [7,8]. This space plays a particularly important role in the drainage of interstitial fluid containing unnecessary substances and waste including β-amyloid from the central grey matter and cerebral cortex [9,10,11,12]. PVMs encounter various substances, including pathogens and waste from blood flow and brain parenchyma, and play a crucial role in regulating inflammatory responses in the CNS [13]. PVMs are the only cells that display constitutive phagocytic potential in the brain parenchyma [14] that and express immunophenotypical markers of activation such as major histocompatibility class II (MHC II), B7, CD40, and Fc receptor (FcR) [3]. Because of their unique localization, phagocytic function and character PVMs are also essential for maintaining blood brain barrier (BBB) function [15].

Research focused on PVM turnover reported that PVMs are partially and continuously replaced under physiological conditions [3]. Under pathological conditions such as rodent experimental allergic encephalomyelitis, there is a great increase in the number of PVMs accumulated around blood vessels in the brain [8]. Previous studies have also suggested that PVMs respond uniquely to particulate matter. In a rat model, carbon particles injected into the cerebral ventricle were move to perivascular spaces and phagocytosed by PVMs within 1 week. Moreover, the carbon could be detected for more than two years in cells that were laden with particles [14]. These data indicated that it is difficult for PVMs to excrete or dispose of carbon particles and that the presence of these particles may induce some signals or responses in the surrounding cells. This evidence suggested that in PVMs and

their surrounding perivascular spaces, particulate substances may stay and promote biological responses over a long period of time.

The authors aimed to investigate the effects of nano-sized particles because previous studies suggested that they have a greater effect than larger sized particles [16,17,18], especially in the CNS [19] and endothelial cells [20,21]. Because of their small size, nano-sized particles have a larger relative surface area per mass than do bulk-size particles of the same material; this feature often makes nano-sized particles more toxic [22]. Small size of nano-sized particles also enables certain nano-sized particles to cross cell membranes and translocate from the environment into the organism [23]. The lungs and airways are the most important exposure sites for involuntary exposure to nano-sized particles. Respirable nano-sized particles not only elicit local pulmonary effects [24,25,26], but they also can translocate from lung epithelium to extrapulmonary organs [27,28] and developing fetus [29]. It has also been reported that maternal exposure to diesel exhaust particles, which contain nano-sized carbon particles at their core, alters the ultrastructure of PVMs and surrounding tissues in the brain of mouse offspring [30]. This finding suggests that maternal exposure to nano-sized particles may alter the phenotype of PVMs and other cerebral cells in mouse offspring.

The aim of the present study was to investigate the effects of maternal exposure to ultrafine carbon black (UfCB) on the perivascular regions, especially the PVMs and astrocytes close to blood vessels in the brains of the offspring of maternally exposed mice (UfCB-exposed offspring).

Materials and Methods

Ultrafine carbon black

Printex 90, purchased from Degussa Ltd. (Frankfurt, Germany), was used as UfCB. The particle is insoluble in water [31]. The manufacturer reported an average primary particle size of 14 nm and an organic impurity content of less than 1%. The specific surface area was determined to be 295-338 m^2/g [32]. The total carbon content measured was >99 wt%, with 0.82 nitrogen and 0.01 hydrogen wt%. Very low levels of both total polycyclic aromatic hydrocarbon (PAH) (74.2 ng/g) [33,34] and total endotoxin (0.142 EU/mg Printex 90) were detected in the sample.

The UfCB particles were suspended at 5 mg/mL in distilled water, sonicated for 30 min, and then filtered through a 450-nm filter (S-2504; Kurabo Co. Ltd., Osaka, Japan) immediately before administration. The particles in the filtered suspension were characterized by transmission electron microscopy (TEM; JEM 1200EXII, JEOL Ltd., Akishima, Tokyo, Japan) on collodion-coated 200 Cu mesh (Nisshin EM, Cat.No. 6511). The size distribution of secondary UfCB particles in the suspension was determined by dynamic light scattering measurement using a NANO-ZS (Sysmex Co., Kobe, Hyogo, Japan) and the Rayleigh-Debye equation. The UfCB concentration in the suspension was calculated to be 95 μg/mL by peak area of carbon signal (2.77 keV) obtained using a field emission scanning electron microscope (JSM-6500F) with an attached energy-dispersive X-ray analyzer (JSM-6500F).

Animals and treatments

Ten pregnant ICR mice (11 weeks of age) were purchased from SLC Inc. (Hamamatsu, Shizuoka, Japan) and were randomly divided into two groups: UfCB-exposed (n = 5) and control (n = 5). The mice were housed under controlled temperature (23±1°C) and humidity (55%±5%) with a 12-hr dark/light cycle and ad libitum access to food and water. The pregnant mice were put into anesthesia box filled with halothane, and then taken out from the box when they began to sleep. The mice were immediately laid on their back and treated with 1 mL/kg (body weight) of UfCB suspension (95 μg/mL, for UfCB group) or distilled water (for control group) by intranasal instillation into both nostrils. 95 μg/mL was maximum concentration of UfCB suspension without bulk agglomeration or any dispersant. The total dose of UfCB (190 μg/kg body weight) was lower than the doses used in many earlier studies of nano-sized particle effects. The treatment were perfomed on gestational days (GDs) 5 and 9, because the fetus of mice on these days is particularly sensitive to various foreign substances in comparison to any other fetal period [35]. Previous study showed that fetal malformation were observed by maternal exposure to single-wall carbon nanotube on GD 5.5 [36]. Additionally, developmental effect of respiratory exposure to UfCB on kidney was examined by twice intranasal instillation on GDs 5 and 9 in the previous study [37]. The number of pups per dam was adjusted randomly to 11 or 12 on postnatal day 1. After weaning at 3 weeks of age, 4–6 male offspring per dam were randomly selected and used for analysis. Brains were collected from male offspring mice at 6 and 12 weeks after birth (Figure 1). All experiments were performed in accordance with Animal Research: Reporting In Vivo Experiments guidelines for the care and use of laboratory animals [38] and were approved by Tokyo University of Science's Institutional Animal Care and Use Committee. All sampling was performed under sodium pentobarbital (50 mg/kg) anesthesia, and all efforts were made to minimize suffering.

Periodic Acid Schiff (PAS) staining

Brains from 6-week-old (n = 5/group) and 12-week-old (n = 5/group) male offspring mice were fixed in 4% paraformaldehyde and 1% glutaraldehyde, embedded in paraffin and cut into 3-μm sections for analysis with PAS staining to visualize PVM granules. The sections were oxidized in 1% periodic acid solution for 1 min. After rinsing for 3 min in distilled water, the sections were soaked in cold Schiff reagent for 45 min. Next, the sections were soaked in sulphurous acid solution 3 times for 5 min and then rinsed for 3 min in distilled water. Finally, the sections were counterstained in haematoxylin for 1 sec, then washed in flowing tap-water, dehydrated in graded alcohol, cleared in xylene, and coverslips were applied with permount mounting medium (Thermo Fisher Scientific Inc., Weltham, MA,USA).

PAS-positive PVM counting

PAS-positive PVMs were observed in sections using a BX-10 microscope (Olympus, Co., Tokyo, Japan) equipped with a digital camera (BX41; Olympus). Fifty sections (total 150 μm) from the longitudinal fissure of the cerebrum along sagittal plane were prepared from each mouse. One in every 10 sections was chosen (every 30 μm) for analysis by PAS staining. In total, 3 sections per mouse (about 150 μm^2/mouse) were subjected to quantitative analysis (Table S1). Stained sections were photographed by optical microscope at 40X magnification. PAS-positive PVM was confirmed by optical microscope with 400X magnification and plotted on 40X-magnified photographs. The PAS-positive cell number per 1 mm^2 area was calculated for each region.

Transmission electron microscopy (TEM)

Brains which removed from 6 (n = 3/group) and 12 (n = 3/group) week-old male offspring mice were fixed by 4% paraformaldehyde and 1% glutaraldehyde. Fixed tissues were washed with phosphate buffer (pH7.4) and post-fixed with osmium tetroxide. These tissue samples were dehydrated in a graded series of ethanol and propylene oxide, and then embedded in

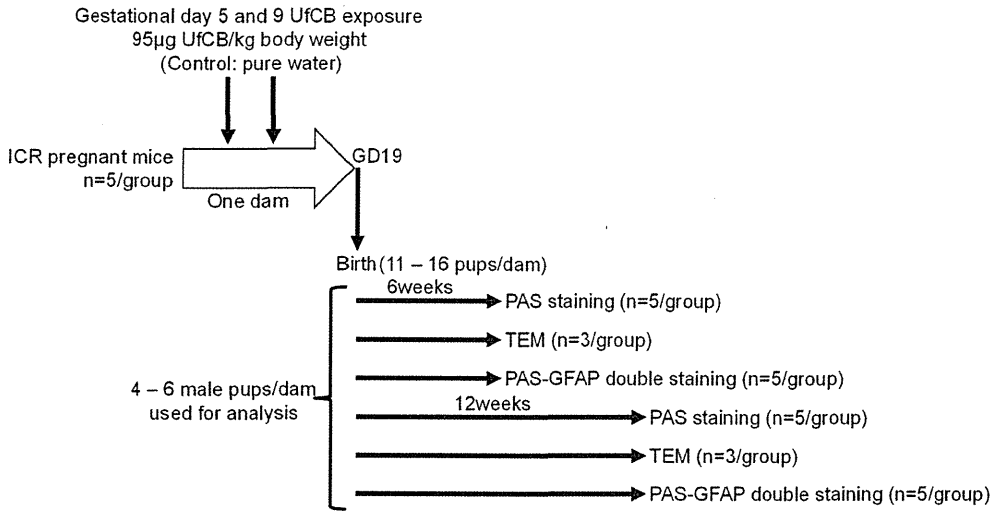

Figure 1. Summarised scheme of animal treatments and sample collection.
doi:10.1371/journal.pone.0094336.g001

epoxy resin (Epon 812, Shell Chemicals Ltd., Houston, TX, USA). Ultrathin sections of each sample were stained with uranyl acetate and lead citrate and examined by transmission electron microscopy (JEOL100-S, JEOL Ltd., Tokyo, Japan) with an accelerating voltage of 80 kV.

Double-staining for GFAP and PAS-positive granules

Brains from 6-week-old (n = 5/group) male offspring mice were used for double-staining for glial fibrillary acidic protein (GFAP) and PAS-positive granules. The brain samples were fixed for 24 hr in 4% paraformaldehyde. Right brains were embedded in paraffin and cut into 6-μm sections for wide-field analysis. Left brains were cryoprotected in phosphate-buffered sucrose solutions (10% sucrose, 4–6 hr; 20% sucrose, 4–6 hr; 30% sucrose, 12–36 hr) with 0.1% sodium azide, embedded in Tissue-Tek OCT compound (Sakura Finetek Japan Co., Ltd., Tokyo, Japan) and then cut into 10-μm frozen sections for observation of detailed morphology.

Visualization of GFAP and PAS-positive granules was performed on paraffin and frozen sections using antibodies and an avidin–biotin-peroxidase method. After blocking endogenous peroxidase and preincubation in 10% normal horse serum, sections were incubated in primary rabbit polyclonal anti-GFAP antibody (Code-No. Z0334, DakoCytomation, Copenhagen, Denmark) diluted 1:1000 in 0.1 M PBS with 0.1% Trion X (PBS-Tx) for 16 hr at 4°C. After rinsing 3 times for 5 min in PBS-Tx, sections were further incubated in secondary biotinylated donkey anti-rabbit IgG (AP182B, Chemicon, Temecula, CA, USA;

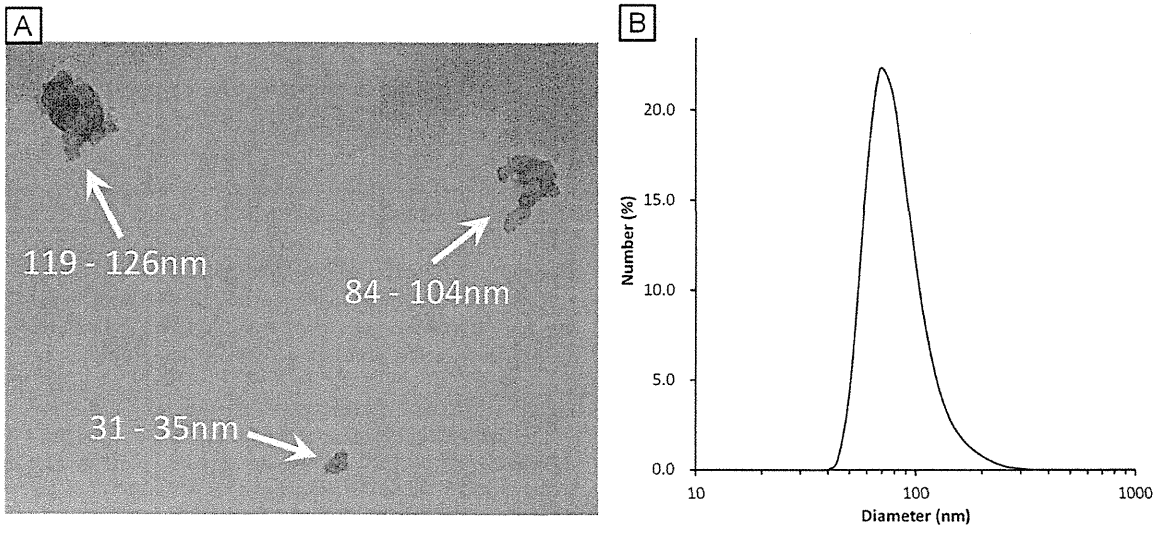

Figure 2. Characterisation of ultrafine carbon black (UfCB). A: Transmission electron microscopy images of UfCB particles in the instillation medium. The yellow numerical value means minor axis - major axis of the secondary UfCB particles. B: Dynamic light scattering data of UfCB in the instillation medium.
doi:10.1371/journal.pone.0094336.g002

Table 1. Number and sex ratio of offspring.

	Number of dams	Number of offspring	Sex ratio (%)*
Control	5	13.8±2.2	46.8±9.8
UfCB	5	13.0±1.2	62.5±21.4

Data are presented as mean ± SD.
*Sex ratio (%) = male/(male + female) ×100
doi:10.1371/journal.pone.0094336.t001

1:1000) for 120 min at room temperature and rinsed 3 times for 5 min in PBS-Tx. The sections were oxidized in 1% periodic acid solution for 3 min, rinsed for 1 min in distilled water, and then soaked in cold Schiff reagent for 60 min. Next, the sections were soaked in sulphurous acid solution 3 times for 3 min and then rinsed for 1 min in distilled water. Finally, the sections were treated with an avidin-biotin-peroxidase complex (Vectastain ABC peroxidase kit, Vector Laboratories Inc., Burlingame, CA, USA; 1:400) for 120 min. The sections were then reacted for peroxidase activity in a solution of 0.02% 3,3′-diaminobenzidene (DAB) in 0.1 M Tris–HCl buffer (pH 7.6) and 0.01% H_2O_2 for 20 min. Immunoreactivity for GFAP was localized to the astrocytic cytoplasm and was visible as light-brown staining. Sections were then washed in 0.1 M PBS, dehydrated in graded alcohol, cleared in xylene, and coverslips were applied with permount mounting medium (Thermo Fisher Scientific).

Statistical analysis

Data are expressed as the mean ± SD. The effects of maternal exposure to UfCB on number and sex ratio of pups at birth were identified by an unpaired t-test, and their body weight at 6 and 12 weeks of age were identified by 2-way ANOVA (Exposure × Age) followed by the Tukey-Kramer post hoc test. For quantitative observation of PAS-positive PVMs, an unpaired t-test was performed. Data analysis was performed using Excel Statistics 2012 for Windows (Social Survey Research Information, Tokyo, Japan). Significance of the difference among means was estimated at $P<0.05$.

Results

UfCB characterisation

The particle suspension (95 μg/mL) was characterised by transmission electron microscopy (TEM) and dynamic light scattering analysis. The TEM analysis of the instillation suspension showed that Printex 90 consisted of open chain-agglomerates of 30–200 nm in diameter (Figure 2A). The filtered Printex 90 suspension, which was employed for intranasal instillation, showed the presence of small agglomerated particles with a peak size of 84.2 nm (Figure 2B). The polydispersity index of 0.143 was low, indicating a narrow size-distribution. This 84.2 nm size corresponds well with the typical small agglomerate sizes of Printex 90 observed under TEM (Figure 2A).

Table 2. Effect of maternal exposure to UfCB on body weight (g) of male offspring at 6 and 12 weeks of age.

	6-week-old male	12-week-old male
Control	33.9±3.0	42.8±3.3
UfCB	33.9±2.1	40.8±5.2

Data are presented as mean ± SD
doi:10.1371/journal.pone.0094336.t002

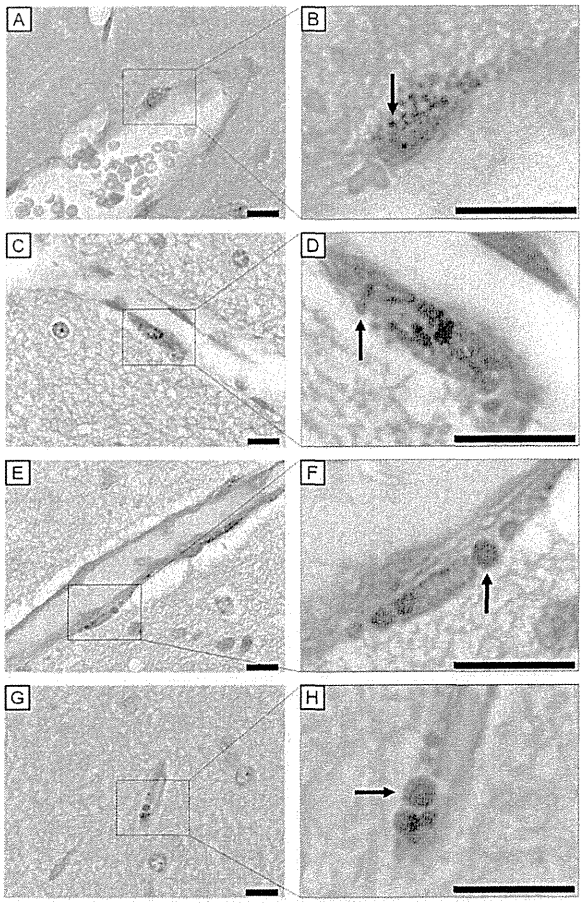

Figure 3. Light micrographs of perivascular macrophages stained with PAS-haematoxylin. All scale bars represent 10 μm. Perivascular macrophages (PVMs) surrounding cerebral blood vessels of (A, B) 6-week-old control mouse, (C, D) 12-week-old control mouse, (E, F) 6-week-old UfCB-exposed offspring mouse, and (G, H) 12-week-old UfCB-exposed offspring mouse were shown. B, D, F, H: Enlarged view of A, C, E and G: PVMs of control mice contained many PAS-positive granules, sized 0.9 μm (B, arrow) and 1.3 μm (D, arrow), in the cytoplasm. Many PAS-positive granules were enlarged in UfCB-exposed offspring (F, arrow: 2.6 μm; H, arrow: 3.0 μm).
doi:10.1371/journal.pone.0094336.g003

Number and body weight of offspring

There was no significant difference between control and UfCB-exposed offspring in number and sex ratio of pups at birth (Table 1) or their body weight at 6 and 12 weeks of age (Table 2).

Light-microscope examination of PAS staining

The intracellular granule, a feature of PVMs, was stained red with PAS [39]. For comparing the general characteristics and contents of PVMs in the offspring of maternally UfCB-exposed mice to control mice, 20 paraffin sections per mouse were observed under a light microscope. The colour photograph shows representative findings for PVMs in both control mice and UfCB-exposed offspring (Figure 3).

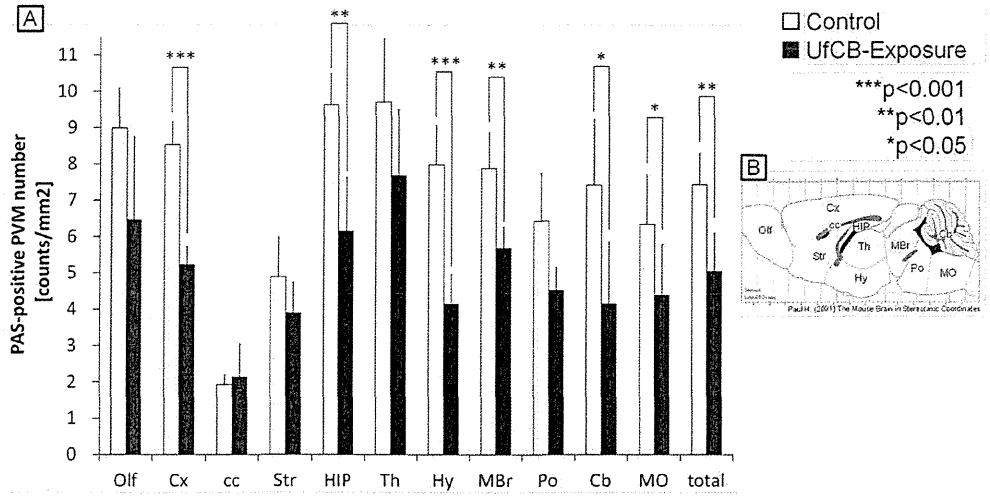

Figure 4. Quantitative observation of PAS-positive PVMs. A: The number of PAS-positive PVMs in each brain region (n = 5/group). Numbers in the following regions were significantly decreased in UfCB-exposed offspring; cerebral cortex (Cx), hippocampus (HIP), hypothalamus (Hy), midbrain (MBr), cerebellum (Cb), and medulla oblongata (MO). Asterisks indicate statistical significance (* $P<0.05$, ** $P<0.01$, *** $P<0.001$). Data are shown as mean ± SD. B: The regions of the brain. Abbreviations: Olf, olfactory bulb; Cx, cerebral cortex; cc, corpus callosum; Str, striatum; HIP, hippocampus; Th, thalamus; Hy, hypothalamus; MBr, midbrain; Po, pons; Cb, cerebellum; MO, medulla oblongata.
doi:10.1371/journal.pone.0094336.g004

In control mice, PVMs were seen exclusively around vessels and located abluminal to endothelial cells in both 6- and 12-week-old offspring (Figure 3A, C). PVMs surrounding cerebral microvessels were slender in shape and contained many PAS-positive granules in their cytoplasm. The diameter of most of the PAS-positive granules was about 1 μm (Figure 3B, D). PAS-positive intracellular inclusions were stained weakly, and the contours of PAS-positive granules were occasionally obscure (Figure 3A, C).

In UfCB-exposed mice, the PVMs were similar in size and shape to those of the control mice, but the diameter of PAS-positive granules was larger (2–3 μm) (Figure 3F, H). Furthermore, the number of PAS-positive granules per PVM was decreased in UfCB-exposed offspring at both 6 weeks and 12 weeks of age (Figure 3F, H).

Quantitative observation of PAS-positive PVMs

For comparing the number of PVMs in UfCB-exposed offspring to control, a total of 15 paraffin sections per group were stained with PAS-haematoxylin and PAS-positive PVMs were counted under a light microscope.

In the control mice, PAS-positive PVMs around vessels numbered 7.42/mm^2 for all regions; in contrast with UfCB-exposed mice where PAS-positive PVMs numbered 5.04/mm^2 (Figure 4, Table S2). The numbers of PAS-positive PVMs were decreased in all regions of the UfCB-exposed offspring except the corpus callosum (cc); the decrease was especially significant in the cerebral cortex (Cx), hippocampus (HIP), hypothalamus (Hy), midbrain (MBr), cerebellum (Cb) and medulla oblongata (MO) (Figure 4).

Ultrastructural observation by transmission electron microscope (TEM)

Since PAS-positive granules morphologically changed and the number of PAS-positive PVMs was decreased in the UfCB group, we observed the ultrastructure of PVMs by TEM. The cerebral arterioles and venules consisted of a thin endothelium and circularly-arranged smooth muscle cells. On the outside of the vessels, the PVMs were situated between astrocytes and endothelial cells.

In control mice, most granules were round, and the contents were homogeneous and high in electron density in both 6- and 12-week-old offspring (Figure 5A, C). There were some inclusion bodies with a vacuolated structure. Only mild swelling of some astrocytic processes and end-feet was observed in the control offspring at both 6- and 12-week-old of age (Figure 5B, C). In UfCB-exposed offspring, granules with honeycomb-like structures were often found in the PVMs in 12-week-old offspring (Figure 5E). Severe swelling of astrocytic end-feet was also found adjacent to the PVMs with denatured granules in 12-week-old offspring (Figure 5E). However, the remarkable change of granules in PVMs and astrocytic end-feet was not observed in the UfCB-exposed offspring 6-week-old offspring. UfCB-like substances were not found in the offspring brains by TEM.

Relationship between PAS-positive granules and astrocytic GFAP expression

Since degeneration of astrocytic end-feet was observed in the UfCB-exposed offspring (Figure 5), we expected that the phenotype of astrocytes contacting with the vasculature was changed; we therefore analysed the expression of GFAP, which is the most commonly used phenotypic marker of astrocytes subset in the CNS, by immunohistochemistry.

In both groups, GFAP-positive astrocytes were focally prominent in the white matter (Figure 6A, C). In UfCB-exposed offspring, however, GFAP-positive astrocytes were clearly detected in the perivascular region of the grey matter (Figure 6C, D). In addition, astrocytic GFAP-positive processes completely surrounded neuronal bodies in the frontal cortex of the grey matter (Figure 6C, D).

GFAP-positive astrocytes were not observed at any sites attached to blood vessels with PVMs with small (approximately 1 μm) PAS-positive granules (Figure 7A), but were found at blood vessels with PVMs that had enlarged (approximately 2–3 μm) PAS-positive granules in the UfCB-exposed offspring (Figure 7B,

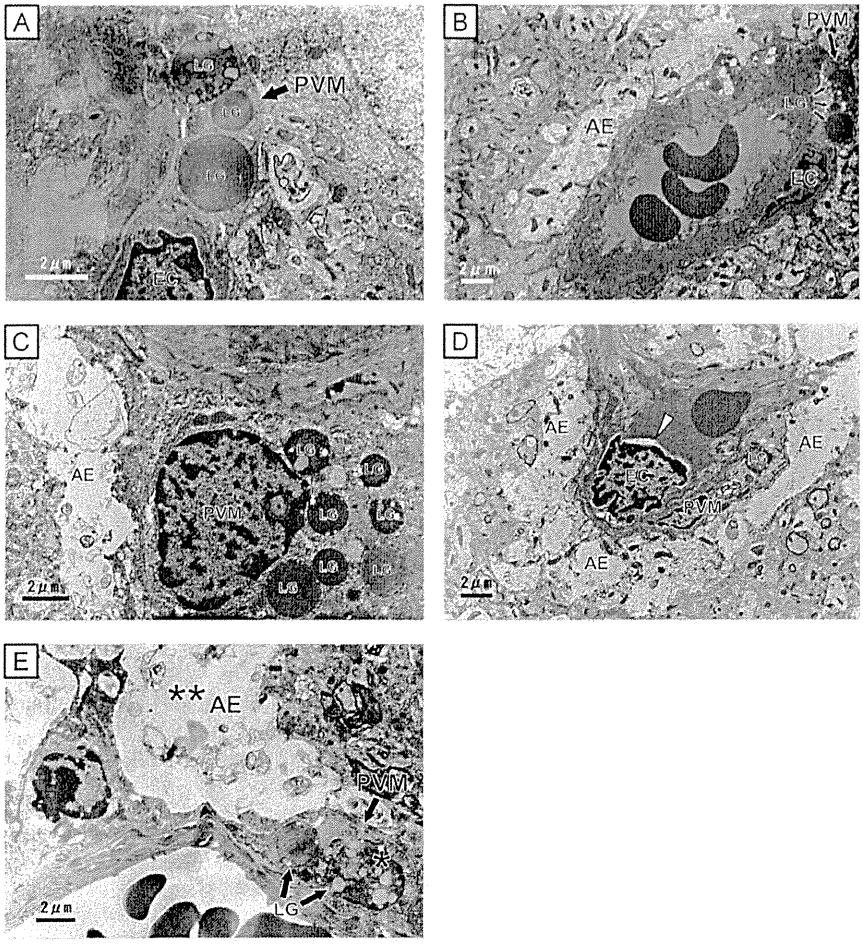

Figure 5. Transmission electron micrographs of perivascular macrophages (PVMs) and astrocytic end-foot. All scale bars represent 2 μm. A–C: Electron micrograph of perivascular regions of the cerebral cortex (grey matter) of (A, B) 6- and (C) 12-week-old mouse in the control group. (A, C) Perivascular macrophages [PVM] were found between endothelial cells and glia limitans with many round lysosomal granules [LG] of moderate intensity and some pale vacuoles. (B, C) The astrocytic end-foot [AE] was attached to a endothelial cells [EC] and a perivascular macrophage. D, E: Electron micrographs of perivascular regions of the cerebral cortex (grey matter) of (D) 6- and (E) 12-week-old UfCB-exposed offspring mouse. (D) Arrow head: Crescent-shaped spaces, an ultrastructural feature of apoptotic bodies [57], of EC were shown. (E) Honeycomb-like structured lysosomal granules (*) were shown in the perivascular macrophages [PVM]. (E) Severe swelling of astrocytic end-feet (**) was found at sites attached to perivascular macrophages with denatured granules.
doi:10.1371/journal.pone.0094336.g005

C). Moreover, GFAP-positive astrocytic end-feet were detected at sites attached to PVMs with enlarged PAS-positive granules (Figure 7E, G, H), and not surrounding PVMs with small PAS-positive granules (Figure 7F, I) around one blood vessel in the UfCB-exposed offspring (Figure 7D–I). These results suggested that the increase in the expression level of GFAP in astrocytic end-feet around blood vessels in the grey matter was correlated with enlargement of PAS-positive granules of PVM.

Discussion

In the present study, we examined the effect of maternal exposure to UfCB on PVMs and surrounding tissue in murine CNS using PAS staining, transmission electron microscopy and GFAP immunohistochemistry. First, we counted PAS-positive PVMs quantitatively in each brain region with a simple method for staining large quantities of tissue sections uniformly and entirely. PAS staining can selectively detect PVMs and meningeal macrophages in the CNS. Only the PAS-positive cells located with blood vessels in the brain parenchyma were counted in order to quantitatively analyse the PVMs in the CNS. Although we can detect murine and human PVMs with scavenger receptors (CD204, CD163) [2,15], these molecules are not so selective because it is also expressed on the microglia in the CNS, especially under inflammatory conditions [15,40]. Previous studies have suggested that PVMs were predominantly present in the grey matter and that the corpus callosum, one of the typical regions in the white matter, had a smaller number of PVMs [1]. The number of PVMs was positively correlated with capillary density in each region. Our quantitative data showed that the frequency of PAS-positive PVM appearance was 4-fold higher in the cerebral cortex than in the corpus callosum; likewise, capillary density was also reported to be about 4-fold higher in the cerebral cortex than in the corpus callosum [41]. PVMs are positive for PAS in physiological and mild-pathologic conditions such as Tay-Sachs

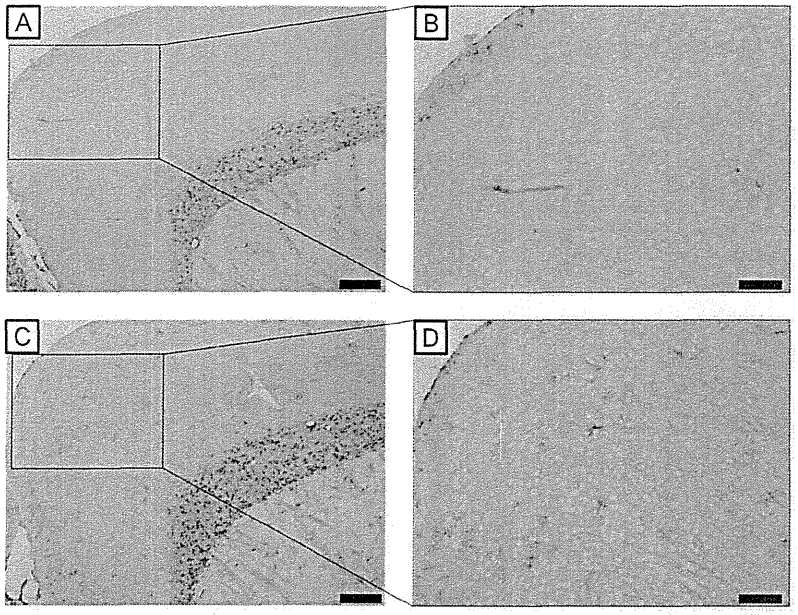

Figure 6. Light micrographs of GFAP-positive astrocytes of the wide-field. Scale bars represent (A, C) 200 m or (B, D) 100 m. A, C: The frontal cortex of 6-week-old male mice of (A) the control group (B) UfCB-exposed offspring. B, D: Enlarged views of A and C. (B) Few GFAP-positive astrocytes were observed in the grey matter in the control group, while (D) many GFAP-positive astrocytes were detected in the grey matter in UfCB-exposed offspring. GFAP-positive astrocytes were not observed at any sites attached to blood vessels with PVMs with small (approximately 1 m) PAS-positive granules (Figure 7A), but were found at blood vessels with PVMs that had enlarged (approximately 2-3 m) PAS-positive granules in the UfCB-exposed offspring (Figure 7B, C). Moreover, GFAP-positive astrocytic end-feet were detected at sites attached to PVMs with enlarged PAS-positive granules (Figure 7E, G, H), and not surrounding PVMs with small PAS-positive granules (Figure 7F, I) around one blood vessel in the UfCB-exposed offspring (Figure 7D-I). These results suggested that the increase in the expression level of GFAP in astrocytic end-feet around blood vessels in the grey matter was correlated with enlargement of PAS-positive granules of PVM .
doi:10.1371/journal.pone.0094336.g006

disease [42], but may be negative for PAS when they are severely degenerated in conditions such as Sandhoff's disease [42]. On the other hand, the number of PVMs are greatly increased and accumulated around blood vessels in experimental allergic encephalomyelitis [8].

Our data showed that PVM granules were enlarged and that the number of PAS-positive PVMs indicated a decrease in "normal" PVMs in a wide area of the CNS after maternal UfCB exposure. Generally, PVM granules are enlarged in mild pathological and aging conditions [42,43,44], presumably by the uptake and accumulation of substances from plasma [43]. More severely denatured PVMs cannot retain spherical (lipid and waste products) granules, and PAS-positive granules have been shown to become negative for PAS-staining [42,45]. These reports suggest that a decrease in PAS-positive PVMs is generally well-correlated with dysfunction of the cells. Furthermore, our electron microscopy results, where some honeycomb-like structures were observed in the granule, support the denaturation of PVM granules after growth (12-week-old offspring) in the UfCB group.

An increase in GFAP expression in the cells surrounding blood vessels in the cerebral cortex suggested that the blood vessels may be damaged in UfCB-exposed offspring. GFAP is an intermediate filament protein, which is the most common phenotypic marker labelling of astrocytes under conditions of denaturation or inflammation [46,47]. Astrocytes highly express GFAP in their end-feet and extend it to injured regions, where cerebral blood vessels or neuronal cells are injured in pathological conditions such as infection and transient ischemia [46,48,49]. In addition, the swelling of astrocytic end-feet in UfCB-exposed offspring, as observed by electron microscopy, was similar to a feature of ischemia-related blood vessel damage [46,47]. These data also suggest that maternal UfCB exposure induces persisting alteration of the phenotype of PVMs and attached astrocytes in the brains of mouse offspring.

Interestingly, the increase in astrocytic GFAP expression level was closely related to the enlargement of granules in the attached PVMs. A decrease in the number of normal PVMs suggests PVM dysfunction in the UfCB group, the cause of which may be the invasion of foreign matter or pathogens to the brain parenchyma [3,43], accumulation of waste products [3], a decrease in immunocompetence in the surrounding blood vessels [3,13], and/or damage to blood vessels and weakening of the BBB function [15]. To protect against and restrict the spread of infectious agents and inflammatory cells in the CNS parenchyma, an astrocyte extends its end-foot to the vessel when there is an increase in the expression level of astrocytic GFAP [46,49]. PVMs with enlarged granules may be associated with the attraction of astrocytic end-feet toward themselves in UfCB-exposed offspring. GFAP-positive astrocytic end-feet were observed around PVMs with enlarged granules.

The present study also contributed to elucidating the mechanism underlying the effect of maternal exposure to ultrafine particles in the atmospheric environment. It is well-known that the core of combustion-derived particles is composed of UfCB [50], which represents relevant surrogate model particles for airborne fine ($PM_{2.5}$) and ultrafine particles [51]. Further investigation is needed to clarify which direct or indirect effect of UfCB is the main contributor to the effect on PVMs and surrounding astrocytes in mouse offspring. Ultrafine particles with a diameter of $<$200 nm may transfer from the pregnant body to offspring by passing through the placenta [29,52] and may directly affect the development of offspring. Alteration in the pregnant body, such as

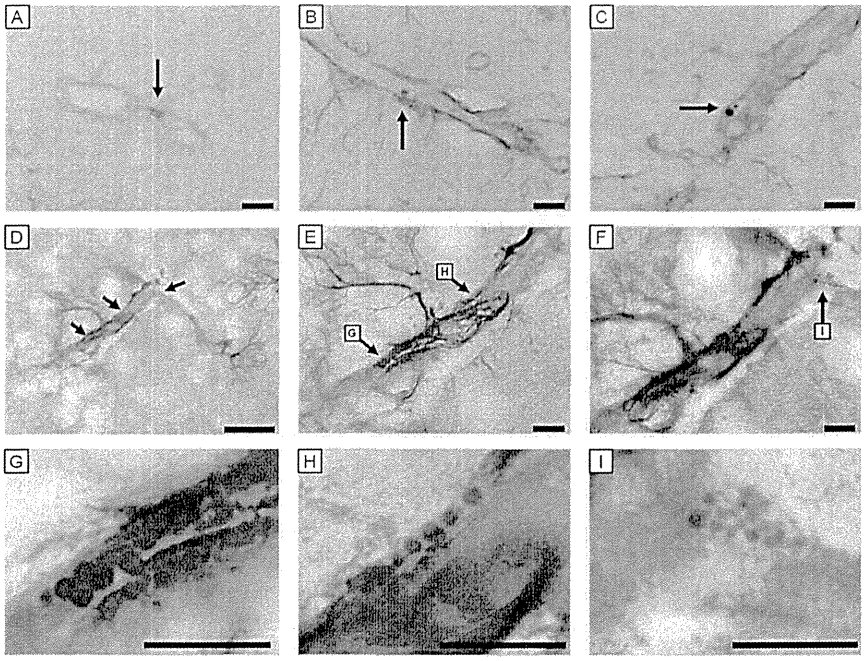

Figure 7. Light micrographs of GFAP-positive astrocytes and PAS-positive PVMs of 6-week-old male mice. All scale bars represent 10 μm. (A–C) 6-μm paraffin sections and (D–I) 10-μm frozen sections. A: PVM surrounding the cerebral blood vessels of a 6-week-old control mouse. GFAP-positive astrocytes were very few in number at sites attached to blood vessels with PVMs with small (approximately 1 μm) PAS-positive granules (arrow). B, C: PVM surrounding cerebral blood vessels of a mouse in the UfCB group. The PVM possessed enlarged granules (arrows). Many GFAP-positive astrocytes were observed at sites attached to PVMs with enlarged granules. D: GFAP-positive astrocytes and PAS-positive PVM (arrows) surrounding cerebral blood vessels of mouse in the UfCB group. E–I: Enlarged views of (D). Around one cerebral vessel, GFAP-positive astrocytic end-feet were detected (E, G, H) at a site attached to PVM with enlarged PAS-positive granules (G, 2.2 μm; H, 1.6 μm), but (F, I) not surrounding PVMs with small PAS-positive granules (smaller than 1.1 μm).
doi:10.1371/journal.pone.0094336.g007

an increase in circulating cytokines or other secondary messengers that are activated in response to inflammation and/or oxidative stress, may also influence the development [53,54,55]. Our results demonstrate the need to find a means of preventing and controlling the developmental effect of maternal exposure to ultrafine particles on the CNS, especially in the maintenance of brain perivascular regions. The previous study reported that the changes of gene expression in olfactory bulb, where is one of the brain region, by exposure to diesel exhaust were prevented by enrichment rearing environment [56]. The living environment during perinatal period is of interest for preventing the development effects of ultrafineparticles.

In summary, the present study showed that exposure of pregnant mothers to UfCB degenerated PVM granules and decreased the number of normal PVMs of offspring. An increase in the expression level of GFAP was also shown in the astrocytes surrounding PVMs with enlarged granules in UfCB-exposed offspring. The phenotypic changes in PVMs and astrocytes indicate that maternal UfCB exposure may alter brain blood vessels and be associated with the risk of brain dysfunction and disorders in future offspring. It would be necessary to clarify the mechanisms underlying the effect of UfCB on the astrocytes and CNS function of offspring.

Supporting Information

Table S1 Total number of PAS-positive PVMs in each sample.
(DOC)

Table S2 Number of PAS-positive PVMs in each brain region. Data are presented as mean ± SD. Abbreviations: Olf, olfactory bulb; Cx, cerebral cortex; cc, corpus callosum; Str, striatum; HIP, hippocampus; Th, thalamus; Hy, hypothalamus; MBr, midbrain; Po, pons; Cb, cerebellum; MO, medulla oblongata.
(DOC)

Author Contributions

Conceived and designed the experiments: KT MU AO. Performed the experiments: AO MS TI. Analyzed the data: AO MU MS. Wrote the paper: AO MU.

References

1. Galea I, Palin K, Newman TA, Van Rooijen N, Perry VH, et al. (2005) Mannose receptor expression specifically reveals perivascular macrophages in normal, injured, and diseased mouse brain. Glia 49:375–384.
2. Kim WK, Alvarez X, Fisher J, Bronfin B, Westmoreland S, et al. (2006) CD163 identifies perivascular macrophages in normal and viral encephalitic brains and potential precursors to perivascular macrophages in blood. Am J Pathol 168:822–834.
3. Williams K, Alvarez X, Lackner AA (2001) Central nervous system perivascular cells are immunoregulatory cells that connect the CNS with the peripheral immune system. Glia 36:156–164.

4. Peters A, Palay SL, Webster HD (1976) The fine structure of thenervous system: the neurons and supporting cells. Philadelphia: WB Saunders.
5. Graeber MB, Streit WJ, Buringer D, Sparks DL, Kreutzberg GW (1992) Ultrastructural location of major histocompatibility complex(MHC) class II positive perivascular cells in histologically normal human brain. J Neuropathol Exp Neurol 51:303–311.
6. Streit WJ, Graeber MB (1993) Heterogeneity of microglial and perivascular cell populations: insights gained from the facial nucleus paradigm. Glia 7:68–74.
7. Lassmann H, Zimprich F, Vass K, Hickey WF (1991) Microglial cells are a component of the perivascular glia limitans. J Neurosci Res 28:236–243.
8. Lassmann H, Schmied M, Vass K, Hickey WF (1993) Bone marrow derived elements and resident microglia in brain inflammation. Glia 7:19–24.
9. Cserr HF, Ostrach LH (1974) Bulk flow of interstitial fluid after intracranial injection of blue dextran 2000. Exp Neurol 45(1):50–60.
10. Weller RO, Kida S, Zhang ET (1992) Pathways of fluid drainage from the brain—morphological aspects and immunological significance in rat and man. Brain Pathol 2(4):277–84.
11. Zhang ET, Richards HK, Kida S, Weller RO (1992) Directional and compartmentalised drainage of interstitial fluid and cerebrospinal fluid from the rat brain. Acta Neuropathol 83(3):233–9.
12. Iliff JJ, Wang M, Liao Y, Plogg BA, Peng W, et al. (2012) A paravascular pathway facilitates CSF flow through the brain parenchyma and the clearance of interstitial solutes, including amyloid β. Sci Transl Med 15;4(147):147
13. Serrats J, Schiltz JC, García-Bueno B, van Rooijen N, Reyes TM, et al. (2010) Dual roles for perivascular macrophages in immune-to-brain signaling. Neuron 65:94–106.
14. Kida S, Steart PV, Zhang ET, Weller RO (1993) Perivascular cells act as scavengers in the cerebral perivascular spaces and remain distinct from pericytes, microglia and macrophages. Acta Neuropathol (Berl) 85:646–652.
15. Fabriek BO, Van Haastert ES, Galea I, Polfliet MM, Döpp ED, et al. (2005) CD163-positive perivascular macrophages in the human CNS express molecules for antigen recognition and presentation. Glia 51:297–305.
16. Donaldson K, Tran L, Jimenez LA, Duffin R, Newby DE, et al. (2005) Combustion-derived nanoparticles: a review of their toxicology following inhalation exposure. Part Fibre Toxicol 21;2:10.
17. Oberdörster G, Oberdörster E, Oberdörster J (2005) Nanotoxicology: an emerging discipline evolving from studies of ultrafine particles. Environ Health Perspect 113(7):823–39.
18. Nel A, Xia T, Mädler L, Li N (2006) Toxic potential of materials at the nanolevel. Science 3;311(5761):622–7.
19. Tin-Tin-Win-Shwe, Yamamoto S, Ahmed S, Kakeyama M, Kobayashi T, et al. (2006) Brain cytokine and chemokine mRNA expression in mice induced by intranasal instillation with ultrafine carbon black. Toxicol Lett 25;163(2):153–60.
20. Vesterdal LK, Folkmann JK, Jacobsen NR, Sheykhzade M, Wallin H, et al. (2010) Pulmonary exposure to carbon black nanoparticles and vascular effects. Part Fibre Toxicol 5;7:33.
21. Peters K, Unger RE, Kirkpatrick CJ, Gatti AM, Monari E (2004) Effects of nano-scaled particles on endothelial cell function in vitro: studies on viability, proliferation and inflammation. J Mater Sci Mater Med 15(4):321–5.
22. Duffin R, Tran L, Brown D, Stone V, Donaldson K (2007) Proinflammogenic effects of low-toxicity and metal nanoparticles in vivo and in vitro: highlighting the role of particle surface area and surface reactivity. Inhal Toxicol 19; 849–856.
23. Stone V, Johnston H, Clift MJ (2007) Air pollution, ultrafine and nanoparticle toxicology: cellular and molecular interactions. IEEE Trans Nanobiosci 6; 331–340.
24. Brown DM, Stone V, Findlay P, MacNee W, Donaldson K (2000) Increased inflammation and intracellular calcium caused by ultrafine carbon black is independent of transition metals or other soluble components. Occup Environ 57, 685–691.
25. Jacobsen NR, Moller P, Jensen KA, Vogel U, Ladefoged O, et al. (2009) Lung inflammation and genotoxicity following pulmonary exposure to nanoparticles in ApoE-/- mice. Part Toxicol. 12; 6, 2.
26. Wilson MR, Lightbody JH, Donaldson K, Sales J, Stone V (2002) Interactions between ultrafine particles and transition metals in vivo and in vitro. Toxicol Appl Pharmacol. 184, 172–179.
27. Oberdörster G, Sharp Z, Atudorei V, Elder A, Gelein R, et al. (2002) Extrapulmonary translocation of ultrafine carbon particles following whole-body inhalation exposure of rats. J Toxicol Environ Health A 65: 1531–1543
28. Kreyling WG, Semmler M, Erbe F, Mayer P, Takenaka S, et al. (2002) Translocation of ultrafine insoluble iridium particles from lung epithelium to extrapulmonary organs is size dependent but very low. J Toxicol Environ Health A 65: 1513–1530
29. Takeda K, Suzuki K, Ishihara A, Kubo-Irie M, Fujimoto R, T, et al. (2009) Nanoparticles transferred from pregnant mice to their offspring can damage the genital and cranial nerve systems. Jounal if Health Science 55(1) 95–102
30. Sugamata M, Ihara T, Takano H, Oshio S, Takeda K (2006) Maternal Diesel Exhaust Exposure Damages Newborn Murine Brains. Journal of Health Science 52:82–84
31. Jackson P, Vogel U, Wallin H, Hougaard KS (2011) Maternal Exposure to Particulate Air Pollution and Engineered Nanoparticles: Reproductive and Developmental Effects. In: Anca, M M, editor. Air Pollution - New Developments. Rijeka University Campus Step Ri. pp. 59–84.
32. Saber AT, Jensen KA, Jacobsen NR, Birkedal R, Mikkelsen L, et al. (2011) Inflammatory and genotoxic effects of nanoparticles designed for inclusion in paints and lacquers. Nanotoxicology 6(5):453–71.
33. Jacobsen NR, Saber AT, White P, Møller P, Pojana G, et al. (2007) Increased mutant frequency by carbon black, but not quartz, in the lacZ and cII transgenes of muta mouse lung epithelial cells. Environ Mol Mutagen 48(6):451–61.
34. Jacobsen NR, White PA, Gingerich J, Møller P, Saber AT, et al. (2011) Mutation spectrum in FE1-MUTA(TM) Mouse lung epithelial cells exposed to nanoparticulate carbon black. Environ Mol Mutagen 52(4):331–7.
35. Wilson JG (1972) Environmental effects on development-teratology. In: N F Affli, edtor. Pathophysiology of gestation, vol. II. New York: Academic. pp. 270–320.
36. Pietroiusti A1, Massimiani M, Fenoglio I, Colonna M, Valentini F, et al. (2011) Low doses of pristine and oxidized single-wall carbon nanotubes affect mammalian embryonic development. ACS Nano. 28;5(6):4624–33.
37. Umezawa M, Kudo S, Yanagita S, Shinkai Y, Niki R, et al. (2011) Maternal exposure to carbon black nanoparticle increases collagen type VIII expression in the kidney of offspring. J Toxicol Sci. 36(4):461–8.
38. Kilkenny C, Browne W, Cuthill IC, Emerson M, Altman DG (2010) Animal research: reporting in vivo experiments: the ARRIVE guidelines. Br J Pharmacol 160: 1577–1579.
39. Mato M, Ookawara S (1979) A simple method for observation of capillary nets in rat brain cortex. Experientia 15;35(4):501–3.
40. Guillemin GJ, Brew BJ (2004) Microglia, macrophages, perivascular macrophages, and pericytes: a review of function and identification. J Leukoc Biol 75(3):388–97.
41. Cavaglia M, Dombrowski SM, Drazba J, Vasanji A, Bokesch PM, et al. (2001) Regional variation in brain capillary density and vascular response to ischemia. Brain Res 10;910(1–2):81–93.
42. Mato M, Takeuchi K, Ookawara S, Yamanaka S, Mashiko T, et al. (2002) Inclusions in novel perivascular macrophages (Mato's fluorescent granular perithelial cells) and neurons in the cerebral cortex of Hex A- and Hex B-deficient mice. Acta Neuropathol 103:119–130.
43. Mato M, Ookawara S, Sakamoto A, Aikawa E, Ogawa T, et al. (1996) Involvement of specific macrophage-lineage cells surrounding arterioles in barrier and scavenger function in brain cortex. Proc Natl Acad Sci U S A 93:3269–3274.
44. Nakazawa T, Yamamura H, Shimizu S, Nishikawa M, Ezaki T, et al. (2006) Acceleration of Age-related Changes in the Granules of Perivascular Macrophages from the Brain of Senescence Accelerated Mice (SAM). J Tokyo Wom Med Univ 76: 82–91.
45. Mato T, Kamei M, Ito R, Sawano M, Inokuchi K, et al. (2009) Beneficial Effects of Cocoa in Perivascular Mato Cells of Cerebral Arterioles in SHR-SP (Izm) Rats. J Clin Biochem Nutr 44:142–150.
46. Sofroniew MV, Vinters HV (2010) Astrocytes: biology and pathology. Acta Neuropathol 119:7–35.
47. Molofsky AV, Krencik R, Ullian EM, Tsai HH, Deneen B, et al. (2012) Astrocytes and disease: a neurodevelopmental perspective. Genes Dev 26:891–907.
48. Klatzo I (1976) Presidental address. Neuropathological aspects of brain edema. J Neuropathol Exp Neurol 1967. 26:1–14.
49. Tsai HH, Li H, Fuentealba LC, Molofsky AV, Taveira-Marques R, et al. (2012) Regional astrocyte allocation regulates CNS synaptogenesis and repair. Science 337(6092):358–62.
50. BéruBé K, Balharry D, Sexton K, Koshy L, Jones T (2007) Combustion-derived nanoparticles: mechanisms of pulmonary toxicity. Clin Exp Pharmacol Physiol 34(10):1044–50.
51. Stoeger T, Takenaka S, Frankenberger B, Ritter B, Karg E, et al. (2009) Deducing in vivo toxicity of combustion-derived nanoparticles from a cell-free oxidative potency assay and metabolic activation of organic compounds. Environ Health Perspect 117(1):54–60.
52. Wick P, Malek A, Manser P, Meili D, Maeder-Althaus X, et al. (2010) Barrier capacity of human placenta for nanosized materials. Environ Health Perspect 118(3):432–6.
53. Hougaard KS, Fadeel B, Gulumian M, Kagan VE, Savolainen KM (2011) Developmental toxicity of engineered nanoparticles. In: Ramesh CG, editor. Reproductive and Developmental Toxicology. Academic Press, San Diego. pp. 269–290.
54. Jackson P, Hougaard KS, Boisen AM, Jacobsen NR, Jensen KA, et al. (2012) Pulmonary exposure to carbon black by inhalation or instillation in pregnant mice: effects on liver DNA strand breaks in dams and offspring. Nanotoxicology 6(5):486–500.
55. Kannan S, Misra DP, Dvonch JT, Krishnakumar A (2007) Exposures to airborne particulate matter and adverse perinatal outcomes: a biologically plausible mechanistic framework for exploring potential. Cien. Saude Colet. 12, 1591–1602.
56. Yokota S, Hori H, Umezawa M, Kubota N, Niki R, et al. (2013) Gene expression changes in the olfactory bulb of mice induced by exposure to diesel exhaust are dependent on animal rearing environment. PLoS One 5;8 (8)
57. Ihara T, Yamamoto T, Sugamata M, Okumura H, Ueno Y (1998) The process of ultrastructural changes from nuclei to apoptotic body. Virchows Arch 433(5):443–7.

J Nanopart Res (2014) 16:2284
DOI 10.1007/s11051-014-2284-7

RESEARCH PAPER

Dose–dependent biodistribution of prenatal exposure to rutile-type titanium dioxide nanoparticles on mouse testis

Miyoko Kubo-Irie · Hiroki Uchida · Shotaro Mastuzawa · Yasuko Yoshida · Yusuke Shinkai · Kenichiro Suzuki · Satoshi Yokota · Shigeru Oshio · Ken Takeda

Received: 19 September 2013 / Accepted: 17 January 2014

Abstract Titanium dioxide nanoparticles (nano-TiO_2), believed to be inert and safe, are used in many products especially rutile-type in cosmetics. Detection, localization, and count of nanoparticles in tissue sections are of considerable current interest. Here, we evaluate the dose–dependent biodistribution of rutile-type nano-TiO_2 exposure during pregnancy on offspring testes. Pregnant mice were subcutaneously injected five times with 0.1 ml of sequentially diluted of nano-TiO_2 powder, 35 nm with primary diameter, suspensions (1, 10, 100, or 1,000 μg/ml), and received total doses of 0.5, 5, 50, and 500 μg, respectively. Prior to injection, the size distribution of nano-TiO_2 was analyzed by dynamic light scattering measurement. The average diameter was increased in a dose–dependent manner. The most diluted concentration, 1 μg/ml suspension, contained small agglomerates averaging 193.3 ± 5.4 nm in diameter. The offspring testes were examined at 12 weeks postpartum. Individual particle analysis in testicular sections under scanning and transmission electron microscopy enabled us to understand the biodistribution. The correlation between nano-TiO_2 doses injected to pregnant mice, and the number of agglomerates in the offspring testes was demonstrated to be dose–dependent by semiquantitative evaluation. However, the agglomerate size was below 200 nm in the testicular sections of all recipient groups, independent from the injected dose during pregnancy.

Keywords Rutile-type nano-TiO_2 · Agglomerates · Dose–dependence · Prenatal exposure · Offspring testis · In-vivo testing · Nanomedicine

M. Kubo-Irie (✉) · H. Uchida · S. Mastuzawa · Y. Yoshida · Y. Shinkai · S. Yokota · K. Takeda
Department of Hygiene Chemistry, Faculty of Pharmaceutical Science, Tokyo University of Science, 2641 Yamazaki, Noda-shi, Chiba 278-8510, Japan
e-mail: miyoko_kubo_irie@hotmail.com

K. Takeda
e-mail: takedak@rs.noda.tus.ac.jp

M. Kubo-Irie
Biological Laboratory, University of the Air, 2-11 Wakaba, Mihama-Ku, Chiba 261-8586, Japan

K. Suzuki · K. Takeda
Center for Environmental Health Science for the Next Generation, Research Institute for Science and Technology, Tokyo University of Science, 2641 Yamazaki, Noda-shi, Chiba 278-8510, Japan

S. Oshio
Department of Hygiene Chemistry, Ohu University School of Pharmaceutical Sciences, 31-1 Misumido, Tomita-machi, Kohriyama-shi, Fukushima 963-8611, Japan

Introduction

Titanium dioxide nanoparticles (nano-TiO_2) are manufactured worldwide in large quantities for use in many products such as paints, plastics, papers, inks,

Published online: 01 February 2014

food colorants, cosmetics, and toothpastes. To evaluate its toxicity, reference substances are required to characterize dose, dimension, and durability (Donaldson et al. 2004; Maynard 2006; Nel et al. 2006; Oberdorster et al. 2005; Soto et al. 2005; Warheit et al. 2008; Yang et al. 2009). As a detection method of nanoparticles, inductively coupled plasma mass spectrometer (ICP-MS) was used to calculate the amount of nanomaterials in organs (De Jong et al. 2008; Fabian et al. 2008; Wang et al. 2007), however, it could not show the localized nanoparticles in the cellular level. Cellular distribution and the effects of nanoparticles analyzed by field emission-scanning electron microscope/energy dispersive X-ray spectroscopy (FE-SEM/EDS) is an issue (Chen et al. 2011; Komatsu et al. 2008; Patri et al. 2009; Umbreit et al. 2011). Transmission electron microscopic (TEM) sections through cells, tissues, and organs for quantifying nanoparticles were reviewed to be efficient (Mayhew et al. 2009).

The effect of nanoparticle exposure and testicular dysfunction have been reported that inhalation to diesel exhaust particles ($\sim 1 \times 10^6$ particles/cm^3, 240 nm with the mass median diameter in the air) during pregnancy reduced daily sperm production (DSP) in adulthood without altering endocrine function or expression in the testes (Hemmingsen et al. 2009), and that maternal airway exposure to nano-TiO_2 (1.7×10^6 particles/cm^3 aerosolized powder, 97 nm of major particle size) was tended to reduce sperm count (Kyjovska et al. 2013) .

In a previous study, we examined the effect of a 400 μg dose exposure of anatase-type nano-TiO_2 (25–70 nm) on pregnant mice by dorsal subcutaneous injection was shown to cause testicular dysfunction in male offspring. The shift of nano-TiO_2 from the mother's body to offspring testis was confirmed by FE-SEM/EDS which showed that these nanoparticles contain Ti by the characteristic peak on 4.51 keV (Takeda et al. 2009). In addition to our previous study, the effects of prenatal exposure to carbon black 200 μg (14 nm) doses administered to pregnant mice were shown to affect reproductive function through damage to the seminiferous epithelium and reduction of DSP in male offspring (Yoshida et al. 2010). These studies have examined the higher doses nanoparticles administered to pregnant mice. Nanomaterials were demonstrated to easily cross the placental barrier with the diameter up to 240 nm in an ex vivo human placental perfusion (Wick et al. 2010) and with that of 70 nm in the 800 μg dose intravenous injection per pregnant mice (Yamashita et al. 2011). It is not currently investigated whether low-dose nanoparticles exposure during pregnancy would effect on the offspring testis.

In this study, we evaluated the dose–dependent biodistribution of prenatal exposure to rutile-type nano-TiO_2 on mice testes in 12-week-old offspring by SEM and TEM.

Materials and methods

Animals

Pregnant ICR mice (2 days postcoitum) were purchased from SLC Co. (Shizuoka, Japan) and divided into four nano-TiO_2 recipient groups and a control group. They were maintained in a temperature- and light-controlled environment (12-h light/12-h dark cycle) with ad libitum access to standard rodent food and water. The treatment and care of all mice were approved by the Animal Care and Use Committee of the Tokyo University of Science.

Characterization of rutile nano-TiO_2

Rutile-type nano-TiO_2 powder of 35 nm with primary diameter was provided by Tayca Co. (Osaka, Japan). The powder was suspended at 1 mg/ml in saline (Otsuka Pharmaceutical Factory Inc., Tokushima, Japan) containing 0.05 % Tween 80 and sonicated for 30 min immediately before subcutaneous injection. Tenfold serial dilutions (1, 10, 100, and 1,000 μg/ml) obtained from the middle layer of the original suspension were prepared to examine the size distribution of nano-TiO_2. Dynamic light scattering (DLS) measurement with Nano-ZS (Sysmex Co., Kobe, Hyogo, Japan) was applied three times for each dose suspension. To observe the dispersed nano-TiO_2 in suspensions, a drop of the suspension was placed on formvar-coated copper grids, which were fully drained off and allowed to air dry. A SEM (JEM-6500F JEOL, Tokyo) with elemental analysis by EDS was used at the same time to identify the presence of Ti element in the seminiferous epithelium. The size and shape of visualized nanoparticles were observed by a JEM 1200EX II TEM (JEOL Ltd., Tokyo, Japan).

Injection of nano-TiO_2

Pregnant mice divided into four nano-TiO_2 recipient groups and control group were injected subcutaneously according to the method described by Sharpe et al. (1998). In the recipient groups, each mouse was injected with 0.1 ml of 1, 10, 100, or 1,000 μg/ml of rutile-type nano-TiO_2 suspension studied in the last section, once each on gestational days 5, 8, 11, 14, and 17. The mice of each group received total doses of 0.5, 5, 50, and 500 μg, respectively. The mice of the control group received 0.1 ml of saline with 0.05 % Tween 80 injected in the same manner. The offspring testes were examined at 12 weeks postpartum.

Semi-quantitative evaluation of the nanoparticles in the seminiferous epithelium by electron microscopy

Three animals were selected (one per litter) for the examination. The dissected testes were directly fixed with 2.5 % glutaraldehyde in 0.2 M sodium cacodylate buffer overnight at 4 °C. After washing in the same buffer, samples were post-fixed in 2 % OsO_4 for 1 h, dehydrated in graded series of ethanol, and embedded in epoxy resin. Ultra-thin (100-nm thickness) sections cut on a Sorvall ultra-microtome MT-2 (Leica Mikrosystem LTD GmbH, Vienna, Austria) for detection of agglomerates in the seminiferous epithelium. Based on SEM and TEM observations of the ultrathin sections adapted from Mayhew et al. (2009), the agglomerates found in a unit (1-μm^2 area) of sections on a grid (200 meshes NISSHIN EM Co. Ltd., Japan) and the number of units on five grids was totalled. The number of agglomerates was then roughly estimated for the 0.5, 5, 50, and 500 μg recipient groups. For ultrastructural observations of the seminiferous epithelium, ultrathin (80 nm thick) sections stained doubly with uranyl acetate and lead citrate.

Results

The nano-TiO_2 injections to pregnant mice

The scheme of rutile-type nano-TiO_2 injections is shown in Fig. 1a. Pregnant mice injected five times with 0.1 ml suspensions received total doses of 0.5, 5, 50, and 500 μg, respectively. The mice delivered their pups on gestational day 19. In the 0, 0.5, 5, 50, and 500 μg recipient groups, the numbers of dams and male to female sex ratios of pups for each group were, respectively, as follows: 4 (dams) and 46 (25 males:21 females); 4 and 52 (26:26); 4 and 56 (27:28); 6 and 69 (40:29); and 5 and 52 (24:28). Pups in each group were weaned on postnatal 21. Male reproductive organs developed fully and no structural malformations were observed. There were no differences observed in general toxicity between the control and the nano-TiO_2-recipient groups during the 12 weeks postpartum.

Characterization of rutile-type nano-TiO_2

The characterization of rutile-type nano-TiO_2 provided by Tayca Co. is shown in Table 1. The most diluted concentration, 1 μg/ml suspensions in saline containing 0.05 % Tween 80, demonstrated that agglomerates with various sizes except few large particles were dispersed well under SEM (Fig. 1b). Under TEM (Fig. 1c) measurement, individual agglomerate below the size around 200 nm were recognized to be spherical or rod shape as a whole and constructed with many nano-TiO_2 particles of 35 nm with primary diameter and held together. The suspensions analyzed using DLS measurement included the intensity-weighted average diameter over all size population (Zeta-average) and the polydispersity index (PDI). The average diameter was increased in a dose–dependent manner; 1–1,000 μg/ml suspensions were from 193.3 ± 5.4 to 1980.3 ± 95.8 nm in diameter (Table and Graph inset in Fig. 1d). Standard deviations of each dose suspension were indicated in the graph. The DLS measurement of the 1 μg/ml suspensions was similar to small agglomerates below 200 nm recognized under SEM (Fig. 1b) and TEM (Fig. 1c).

Detection of rutile-type nano-TiO_2 in the testicular sections of offspring at 12 weeks

At high magnification under TEM, some unambiguous electron dense particles were found in the Sertoli cell cytoplasm of the 0.5 μg recipient group (Fig. 2a). There were loose adhesions around the Sertoli cell with many vacuoles and a deformed sperm nucleus with a part of uncondensed chromatin. To confirm

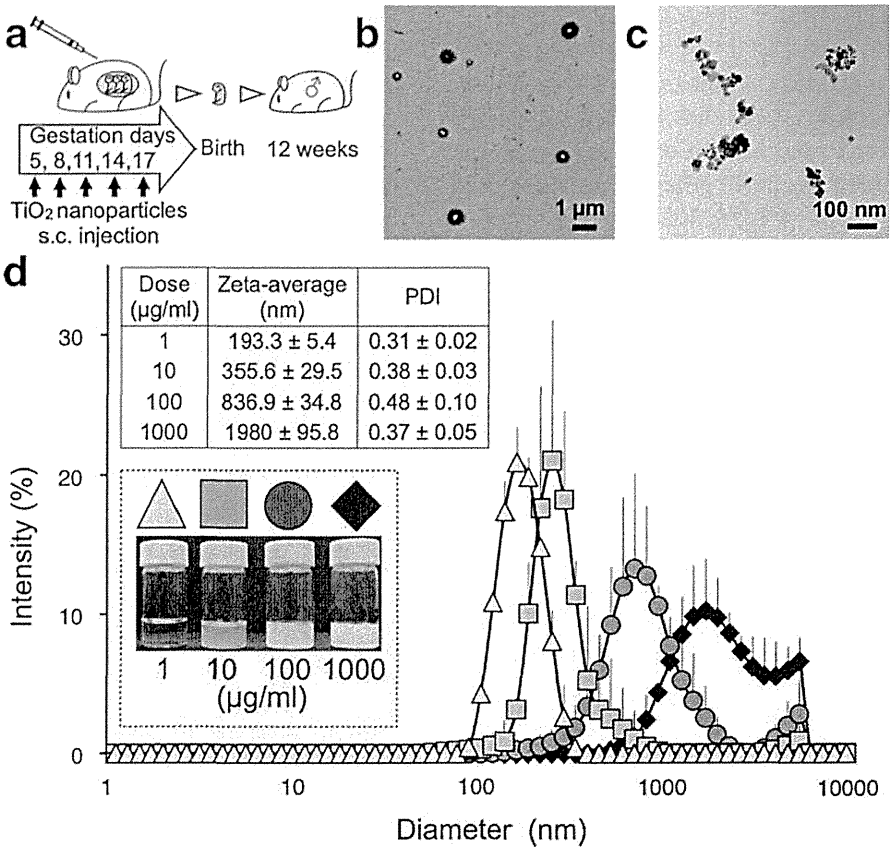

Fig. 1 Scheme of nano-TiO_2 injection and characterization of nano-TiO_2 dosage suspensions. **a** Subcutaneous injection into pregnant ICR mice; 0.1 ml of 1, 10, 100, or 1,000 μg/ml of rutile-type nano-TiO_2 dose on gestational days 5, 8, 11, 14, and 17. The mice of each group received total doses of 0.5, 5, 50, and 500 μg, respectively. **b** SEM images of many small agglomerates below 200 nm dispersed in the most diluted 1 μg/ml suspension. **c** TEM image, with 10 times higher magnification than SEM image, indicates spherical or rod shapes agglomerates below 200 nm are composed of spherical TiO_2 with primary diameter around 35 nm in the same suspension. **d** Characterization of nano-TiO_2 suspensions of tenfold serial dilutions. The diluted solution with 0.05 % Tween 80 to 1, 10, 100, or 1,000 μg/ml analyzed by DLS. The intensity-weighted average diameter over all size population (Zeta-average) and the PDI were shown in Table *inset*. The average diameter was increased in a dose–dependent manner

Table 1 Characterization of rutile-type TiO_2 powder provided by Tayca Co.

Appearance	White powder
TiO^2 (%)	Min 96
pH	Neutral
Cristal structure	Rutile
Property of surface	Hydrophilic
Particle size (nm)	35
Specific surface area	30–50 (m^2/g)

whether the particles contained the Ti element or not, FE-SEM/X-ray spectroscopy were performed to localize nano-TiO_2 (Fig. 2b) and the X-ray spectrum indicated the contain Ti by the characteristic peak on 4.51 keV in the same observed particles (Fig. 2c). The small agglomerate composed of some nano-TiO_2 was found in the Sertoli cell cytoplasm of the 5 μg recipient group. Sertoli cells demonstrated phagocytic functions which suggested that multivesicular vesicles contained damaged mitochondria and small vesicles (Fig. 2d). The small agglomerate was also located in the cytoplasm of the spermatid in the 50 μg recipient group (Fig. 2e) and was positioned beside a developing acrosome enveloped a part of the mid-spermatid nucleus with dispersed chromatin in 500 μg recipient group (Fig. 2f). This indicated that the small agglomerate in the seminiferous epithelium was composed of

nano-TiO_2 35 nm in primary diameter in across all recipient groups. A correlation between nano-TiO_2 doses injected to pregnant mice, and the number of agglomerates in the seminiferous epithelium was demonstrated by the semi-quantitative evaluation (Fig. 2g).

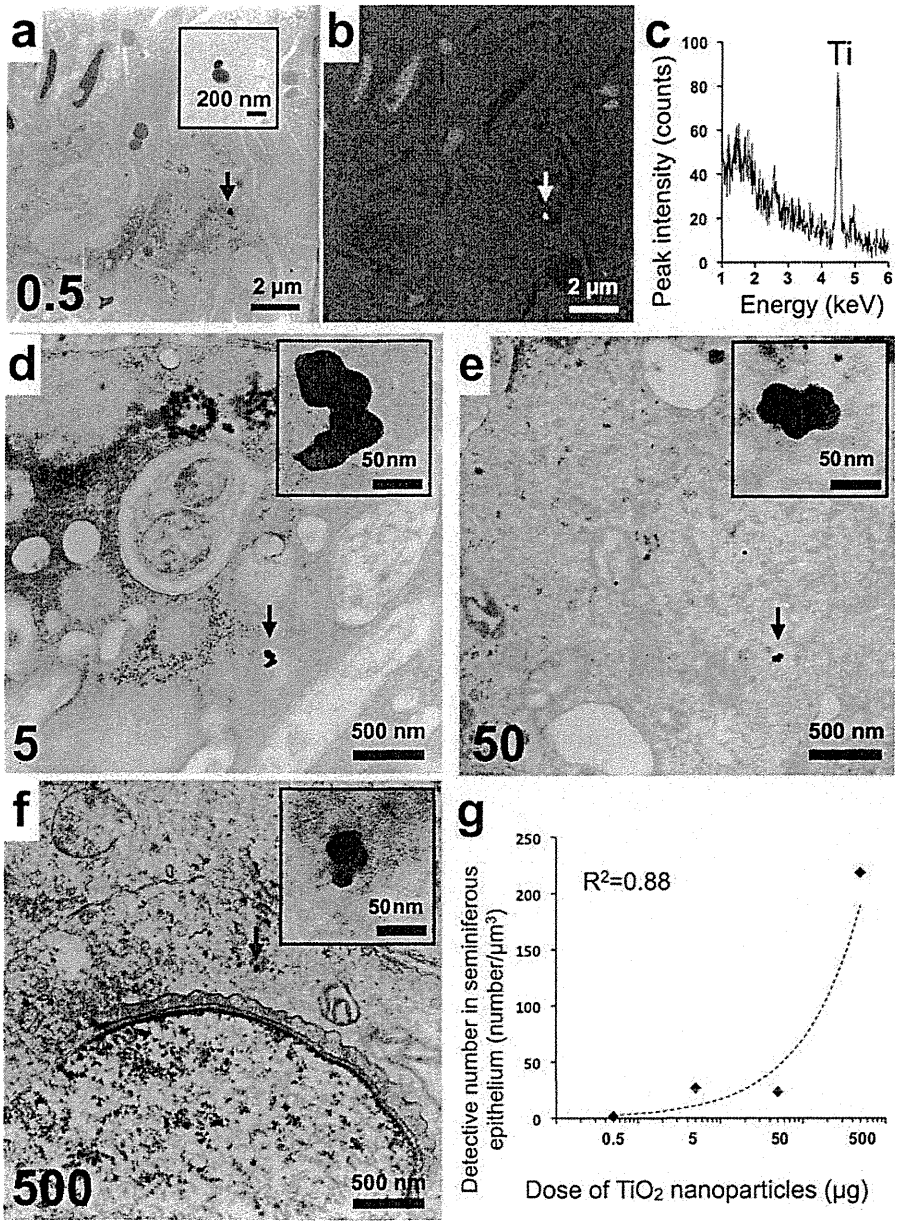

Fig. 2 Nano-TiO_2 in the seminiferous epithelium. **a** TEM image of the seminiferous epithelium in the 0.5 μg group. A *black arrow* shows electron dense particles in the Sertoli cell. The *inset* indicates a small agglomerate of a few nanoparticles. **b** SEM images of the same TEM micrograph. A *white arrow* shows the same agglomerate. **c** X-ray spectrometry indicates Ti peaks on 4.51 keV in the same agglomerate. This observation revealed nano-TiO_2 transferred from pregnant mice to offspring testes. **d** The small agglomerate (*black arrow*) in the cytoplasm of Sertoli cell in the 5 μg group. The *inset* indicates the agglomerate of nano-TiO_2. **e, f** The agglomerate (*black arrow*) in the cytoplasm of spermatids in the 50 and 500 μg groups. The *inset* shows the agglomerate of nano-TiO_2. **g** Semi-quantitative evaluation of the nano-TiO_2 in the seminiferous epithelium. The standard curve shows the dose–dependent relationship when nano-TiO_2 are injected at sufficiently high doses

Ultrastructural observations

Electron microscopic observations were performed to examine the seminiferous epithelium in greater detail. In the control group, spermatogenesis advanced normally with spermatogenic cells orientated from the basal to the adluminal compartment and mature spermatozoa were individually released from Sertoli cells into the adluminal lumen (spermiation). Sertoli cells regularly positioned at the basement membrane had a large nucleus with a few nucleoli and the cytoplasm closely contacted the neighboring spermatogenic cells (Fig. 3a). In the 0.5 μg recipient group, a cluster of mature sperm enveloped by the Sertoli cell cytoplasm was positioned at the basal compartment (Fig. 3b). Similar sperm heads at the basal compartment were observed in the other doses recipient groups. Loose adhesion between spermatogenic cells was found in the seminiferous epithelium in the 5 and 50 μg recipient groups (Figs. 3c, d). In the 500 μg recipient group, the sperm head covered irregularly with acrosome was found. The cytoplasm of Sertoli cell around sperm heads showed vacuolization with many electron dense vesicles (Fig. 3e).

In the adluminal lumen, Sertoli cells engulfed a sperm head with an elongated acrosome and two

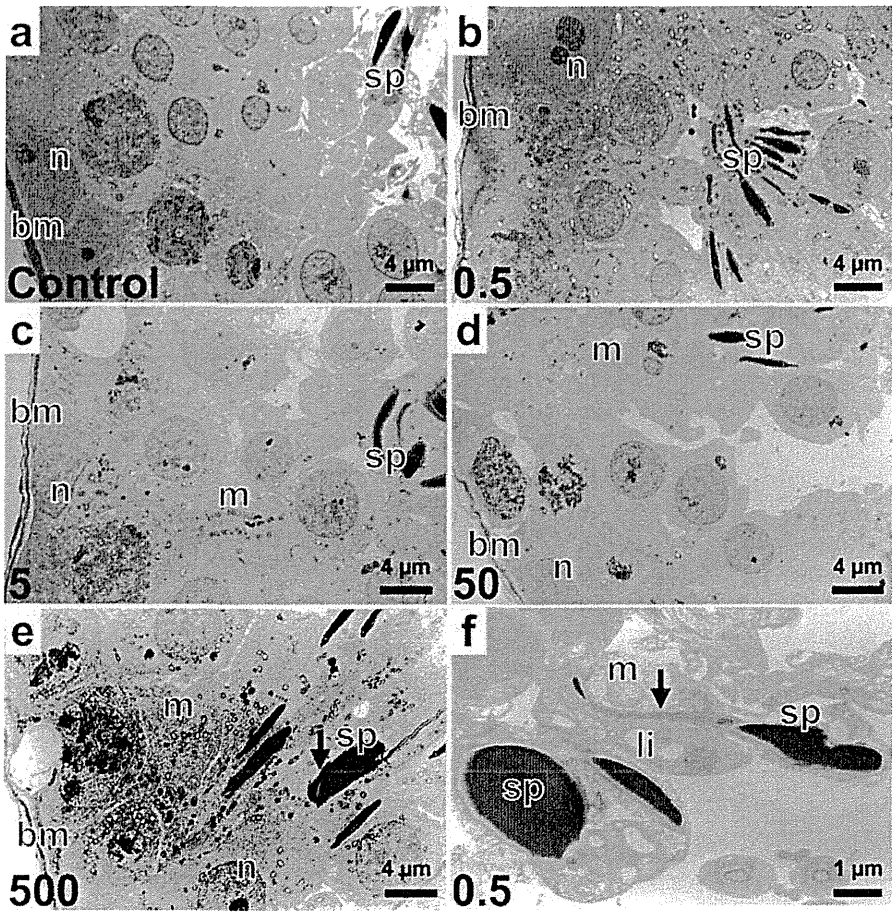

Fig. 3 Ultrastructural alteration of the seminiferous epithelium. **a** Control group: mature spermatozoa released individually into the lumen (spermiation). The Sertoli cell was positioned at the basement membrane and the cytoplasm closely contacted the neighboring spermatogenic cells. **b**, **c** A cluster of mature sperm nuclei located at the basal compartment in the 0.5 and 5 μg groups. **d** The Sertoli cell lost cell adhesion between the neighboring spermatogenic cells in the 50 μg group. **e** A sperm head irregularly covered with acrosome (*black arrow*) was located at the basal compartment. Sertoli cells around sperm heads showed vacuolization in the 500 μg group. **f** An abnormal sperm head with elongated acrosome (*black arrow*) in the 0.5 μg group. The cytoplasm engulfed sperm nuclei had many lipid droplets, Golgi body, and collapsed cristae of mitochondria. *bm* basement membrane, *li* lipid droplets, *m* mitochondria, *n* Sertoli cell nucleus, *sp* mature sperm head